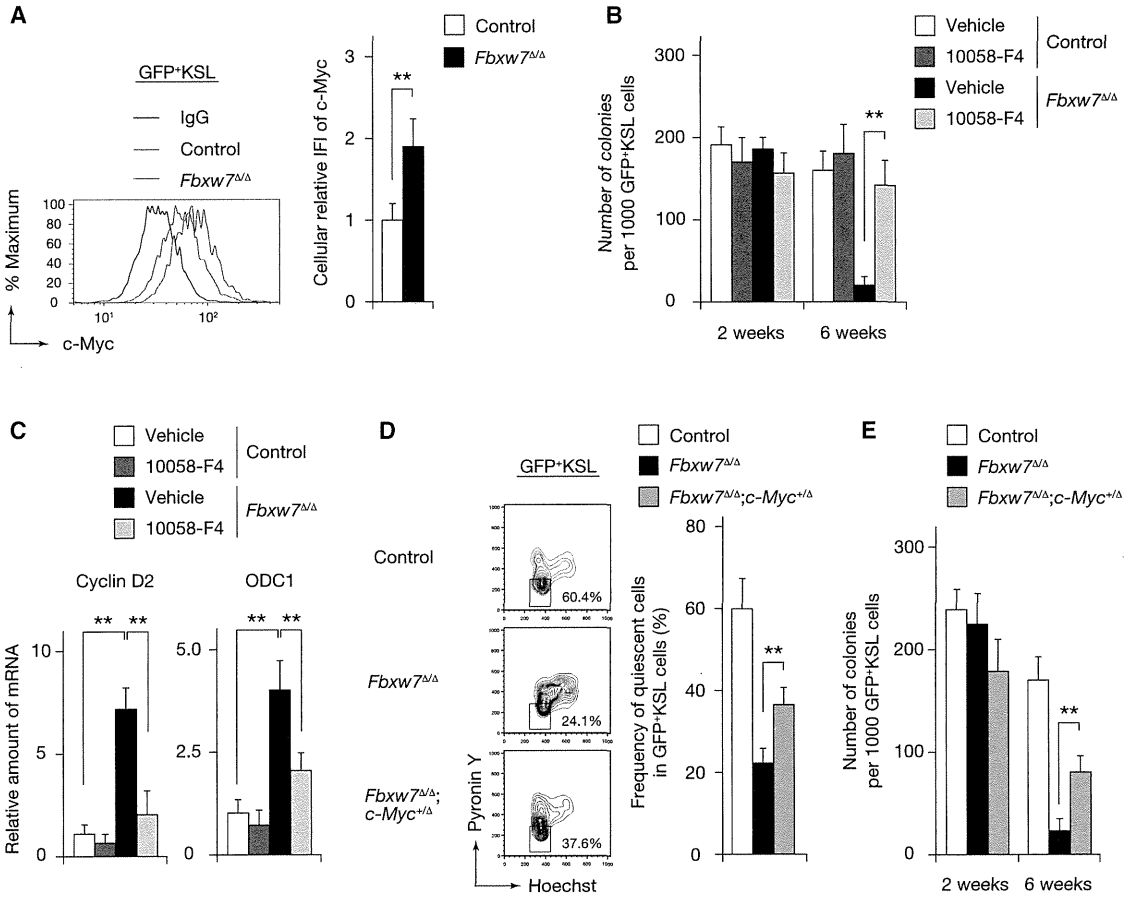

Figure 3. Inhibition of c-Myc Rescues the Phenotype of Fbxw7-Deficient LICs

(A) The abundance of c-Myc in *Fbxw7*$^{\Delta/\Delta}$ or control GFP$^+$KSL cells from mouse recipients of the first BMT was measured by flow cytometry (left panel). Relative c-Myc immunofluorescence intensity (IFI) was determined (n = 5) (right panel). IgG, immunoglobulin G.

(B) Colony formation by *Fbxw7*$^{\Delta/\Delta}$ and control LICs after culture for 2 or 6 weeks with or without 10058-F4 (n = 5).

(C) Control and *Fbxw7*$^{\Delta/\Delta}$ LICs were assayed for cyclin D2 and ODC1 mRNAs by RT and real-time PCR analysis after culture on OP-9 cells for 2 weeks with or without 10058-F4 (n = 5).

(D) The percentage of quiescent cells among GFP$^+$KSL cells was determined for control, *Fbxw7*$^{\Delta/\Delta}$, or *Fbxw7*$^{\Delta/\Delta}$;*c-Myc*$^{+/\Delta}$ bone marrow cells from recipients (n = 5) of the first BMT.

(E) Colony formation by BCR-ABL-transduced KSL cells of the indicated genotypes after 2 or 6 weeks of culture on OP-9 cells (n = 3).

Data are means ± SD. **p < 0.01. See also Figure S3.

Loss of Fbxw7 in LICs Induces Apoptosis in a p53-Dependent Manner

Given that deregulation of c-Myc activation often triggers apoptosis in a p53-dependent manner (Matsuoka et al., 2008; Onoyama et al., 2007), we postulated that p53-dependent apoptosis might be induced by accumulation of c-Myc in Fbxw7-deficient LICs and contribute to LIC exhaustion. The proportion of apoptotic cells did not differ significantly between control and Fbxw7-deficient LICs isolated from recipients of the first BMT. However, the frequency of annexin V$^+$ apoptotic cells was markedly greater among *Fbxw7*$^{\Delta/\Delta}$ GFP$^+$KSL cells than among control GFP$^+$KSL cells from recipients of the second BMT, whereas such a difference was not apparent for leukemic progenitors (Figure 4A). To determine whether this apoptosis in Fbxw7-deficient LICs is induced in a p53-dependent manner, we next cultured control or *Fbxw7*$^{\Delta/\Delta}$ GFP$^+$KSL cells isolated from recipients of the first BMT with the p53 inhibitor pifithrin-α (PFTα) (Komarov et al., 1999). Analysis of colony formation revealed that the exhaustion apparent in *Fbxw7*$^{\Delta/\Delta}$ GFP$^+$KSL cells after 6 weeks of culture was efficiently inhibited by treatment of the cells with PFTα (Figure 4B). To confirm that PFTα indeed inhibits p53 function in these cells, we measured the abundance of mRNAs for p21 and Noxa, the genes for which are direct targets of p53. The amounts of these mRNAs were increased in Fbxw7-deficient LICs compared with those in control cells, and each increase was attenuated by treatment with PFTα (Figure 4C), suggesting that PFTα indeed inhibits p53 activity in these cells. To further show that Fbxw7 deficiency in LICs induces apoptosis in a p53-dependent manner, we generated Mx1-Cre;*Fbxw7*$^{F/F}$;*p53*$^{-/-}$ mice in order to determine the proportion of apoptotic cells and colony-forming ability for *Fbxw7*$^{\Delta/\Delta}$;*p53*$^{-/-}$ LICs. The increase in the frequency of apoptosis apparent for Fbxw7-deficient LICs from recipients of the second BMT was not observed with *Fbxw7*$^{\Delta/\Delta}$;*p53*$^{-/-}$ LICs

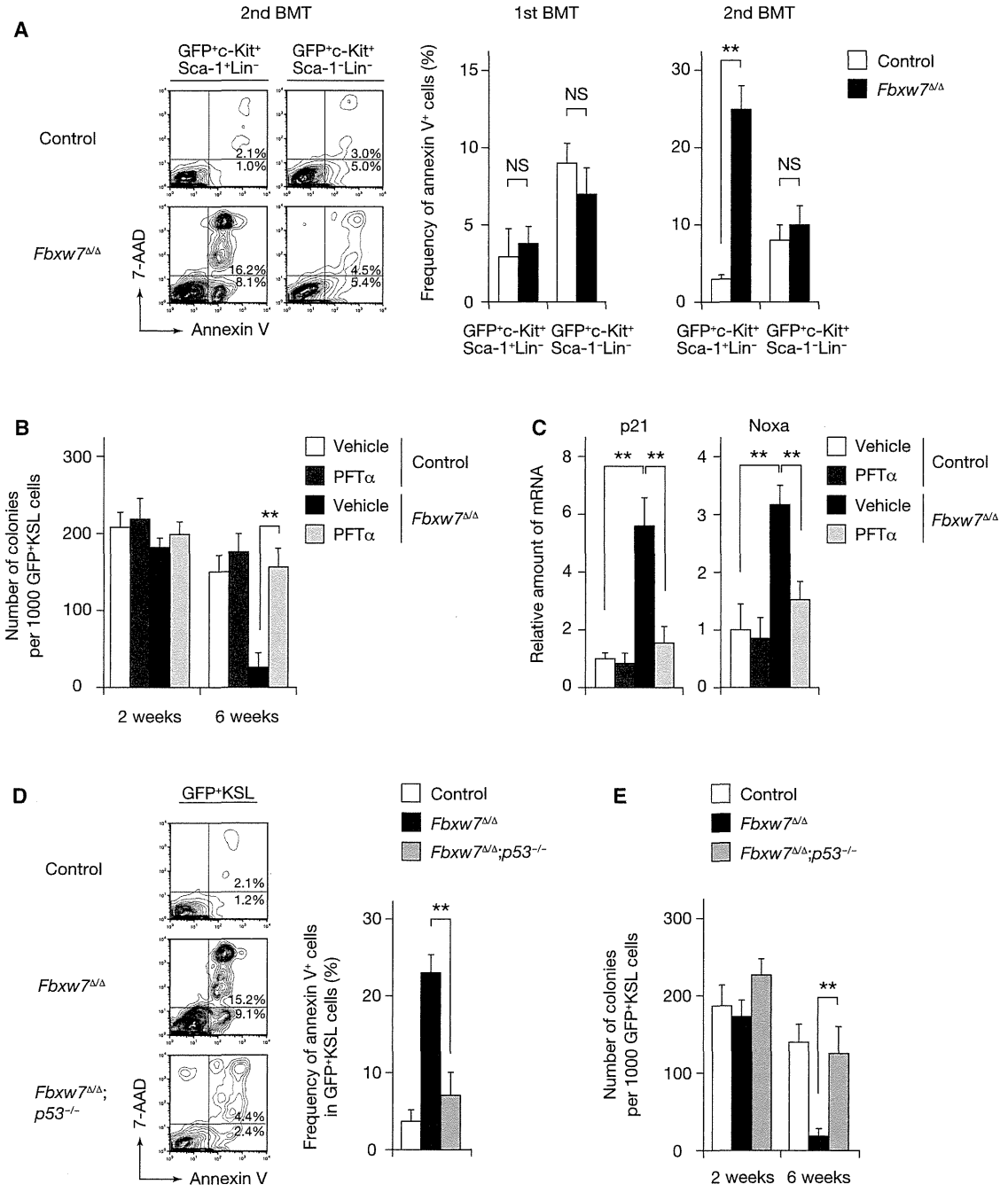

Figure 4. Apoptosis Is Induced in Fbxw7-Deficient LICs in a p53-Dependent Manner

(A) The frequency of annexin V$^+$ cells among *Fbxw7*$^{\Delta/\Delta}$ and control cells of the indicated fractions from mouse recipients (n = 3) of the first or second BMT was determined by flow cytometry. 7-AAD, 7-aminoactinomycin D.

(B) Colony formation by *Fbxw7*$^{\Delta/\Delta}$ and control LICs after culture for 2 or 6 weeks with or without PFTα (n = 5).

(C) Control and *Fbxw7*$^{\Delta/\Delta}$ LICs were assayed for p21 and Noxa mRNAs by RT and real-time PCR analysis after culture on OP-9 cells for 2 weeks with or without PFTα (n = 5).

(D) The proportion of annexin V$^+$ cells among GFP$^+$KSL cells was determined by flow cytometry for control, *Fbxw7*$^{\Delta/\Delta}$, or *Fbxw7*$^{\Delta/\Delta}$;*p53*$^{-/-}$ bone marrow cells from recipients (n = 3) of the second BMT.

(E) Colony formation by cells of the indicated genotypes after culture for 2 or 6 weeks on OP-9 cells (n = 3).

Data are means ± SD. **p < 0.01; NS, not significant.

(Figure 4D). Consistent with this finding, the decrease in the number of colonies derived from Fbxw7-deficient LICs after 6 weeks of culture on OP-9 cells was reversed by deletion of the p53 gene (Figure 4E). Collectively, these results indicated that Fbxw7 deficiency in LICs results in deregulated c-Myc activation, impaired maintenance of quiescence, subsequent apoptosis as a result of p53 induction, and consequent cell exhaustion.

The Combination of Fbxw7 Ablation and Anticancer Drug Treatment Is Effective for LIC Eradication

Although our results implicated Fbxw7 as a potential target for leukemia therapy, the timing of CML development and the survival rate did not differ between the recipients of the first BMT harboring control or Fbxw7-deficient LICs (Figures 2E and 2G), suggesting that inhibition of Fbxw7 alone would not suffice as an effective therapy for CML. To address this problem, we examined the effects of combining Fbxw7 ablation with imatinib. Recipients of the first BMT were injected with pIpC on 7 alternate days beginning the day after transplantation and were then administered imatinib twice a day at 100 mg/kg for 2 weeks beginning 20 days after transplantation (Figure 5A). Determination of the proportion of annexin V^+ cells among GFP^+KSL cells revealed that the frequency of apoptosis among imatinib-treated *Fbxw7*$^{\Delta/\Delta}$ LICs was significantly greater than that among imatinib-treated control LICs (Figure 5B), indicating that Fbxw7-deficient LICs are sensitive to imatinib. In contrast, imatinib was able to efficiently induce apoptosis in both control and Fbxw7-deficient leukemic progenitors and bulk leukemic cells. The number of colonies formed by imatinib-treated *Fbxw7*$^{\Delta/\Delta}$ GFP^+KSL cells was smaller than that formed by vehicle-treated *Fbxw7*$^{\Delta/\Delta}$ GFP^+KSL cells or by imatinib-treated control GFP^+KSL cells (Figure 5C).

Analysis of the effects of this combination therapy on CML development in vivo revealed that it markedly reduced the number of Fbxw7-deficient LICs (Figure 5D). Consistent with these findings, most mice treated with imatinib alone showed a moderate delay in the onset of disease but developed CML after discontinuation of imatinib (Figure 5E), dying within 60 days after BMT (Figure 5F). In contrast, combination therapy with Fbxw7 ablation and imatinib resulted in a marked attenuation of CML development that remained apparent even after discontinuation of imatinib treatment (Figures 5E and 5F). Furthermore, when LICs isolated from recipients of the first BMT were transplanted into new recipients, we found that, whereas LICs treated with imatinib alone still had the potential to confer disease, an apparently complete cure was achieved in all recipients of LICs treated with the combination therapy of Fbxw7 ablation and imatinib (Figure 5F). These results indicated that the effectiveness of the combination therapy is attributable to disrupted maintenance of LICs. We also combined *Fbxw7* deletion and treatment with the conventional anticancer drug cytosine arabinoside (Ara-C) and obtained similar results (Figures S4A–S4D). Analysis of signaling downstream of BCR-ABL in GFP^+KSL cells isolated from recipients of the first BMT at 36 days after transplantation revealed no differences in the proportions of cells expressing phosphorylated forms of Stat5, Crkl, or Akt between imatinib-treated control and *Fbxw7*$^{\Delta/\Delta}$ LICs (Figures S4E–S4G). Collectively, these data thus suggested that LICs whose quiescence is interrupted by Fbxw7 loss are actively cycling and thus sensitive to imatinib or Ara-C treatment and that these combination therapies of Fbxw7 ablation and anticancer drug administration are able to eradicate LICs and provide a survival advantage compared with currently available treatments.

Fbxw7 Deficiency Affects LICs More than It Does Normal HSCs

Given that Fbxw7 is essential for maintenance of both HSCs and LICs, the targeting of LICs by Fbxw7 ablation combined with anticancer drugs might also be expected to damage HSCs. We thus compared the sensitivity of HSCs and LICs to Fbxw7 ablation. To this end, we infected KSL cells from control or Mx1-Cre;*Fbxw7*$^{F/F}$ mice with the retrovirus encoding the $p210^{BCR-ABL}$ oncoprotein and GFP (to yield LICs) or with a virus encoding GFP alone (to yield HSCs) and then transplanted the cells into recipient mice. GFP^+KSL cells from these mice were subsequently transferred to new recipients, which were then injected with pIpC (Figure 6A). Analysis of GFP^+KSL cells from these latter recipients revealed that exit from quiescence induced by Fbxw7 ablation was more pronounced for LICs than for HSCs (Figure 6B). Accordingly, whereas the proportion of apoptotic cells among LICs did not differ from that among HSCs isolated from recipients of the first BMT, it was greater for Fbxw7-deficient LICs than for Fbxw7-deficient HSCs isolated from recipients of a second BMT (Figure 6C). Consistent with these results, whereas Fbxw7 deficiency did not affect the number of HSCs or LICs in recipients of the first BMT, it reduced the number of LICs to a greater extent than it did that of HSCs in recipients of the second BMT (Figure 6D).

To examine the mechanism underlying this difference in sensitivity to Fbxw7 deficiency between HSCs and LICs, we first compared the amount of Fbxw7 mRNA in these cells. RT and real-time PCR analysis revealed that the abundance of Fbxw7 mRNA in LICs was more than twice that in HSCs (Figure S5A). Given that such an increase in the amount of Fbxw7 mRNA was not observed in KSL cells expressing a kinase-dead (K1176R) mutant of BCR-ABL (Zhang and Ren, 1998), the upregulation of Fbxw7 mRNA in LICs is likely attributable to BCR-ABL kinase activity. The level of c-Myc mRNA was also markedly increased in LICs compared with that in HSCs or in KSL cells expressing the kinase-dead mutant of BCR-ABL (Figure S5B), and intracellular flow cytometric analysis revealed that the abundance of c-Myc in LICs was about five times that in HSCs or in KSL cells expressing the BCR-ABL mutant (Figure S5C). We also confirmed that these effects of BCR-ABL on KSL cells were reversed by imatinib treatment (Figures S5A–S5C). We further examined whether the difference in sensitivity to Fbxw7 deficiency between HSCs and LICs might be attributable to the difference in the abundance of c-Myc in these cells. Both exit from quiescence and apoptosis induced by *Fbxw7* deletion were more pronounced in HSCs overexpressing c-Myc and were less pronounced in *c-Myc*$^{+/\Delta}$ HSCs, than in control HSCs (Figures S5D and S5E). Accordingly, the decrease in the number of stem cells induced by Fbxw7 ablation in recipients of the second BMT was greater for HSCs overexpressing c-Myc, and smaller for *c-Myc*$^{+/\Delta}$ HSCs, than for control HSCs (Figure S5F). We next compared sensitivity to combination therapy with

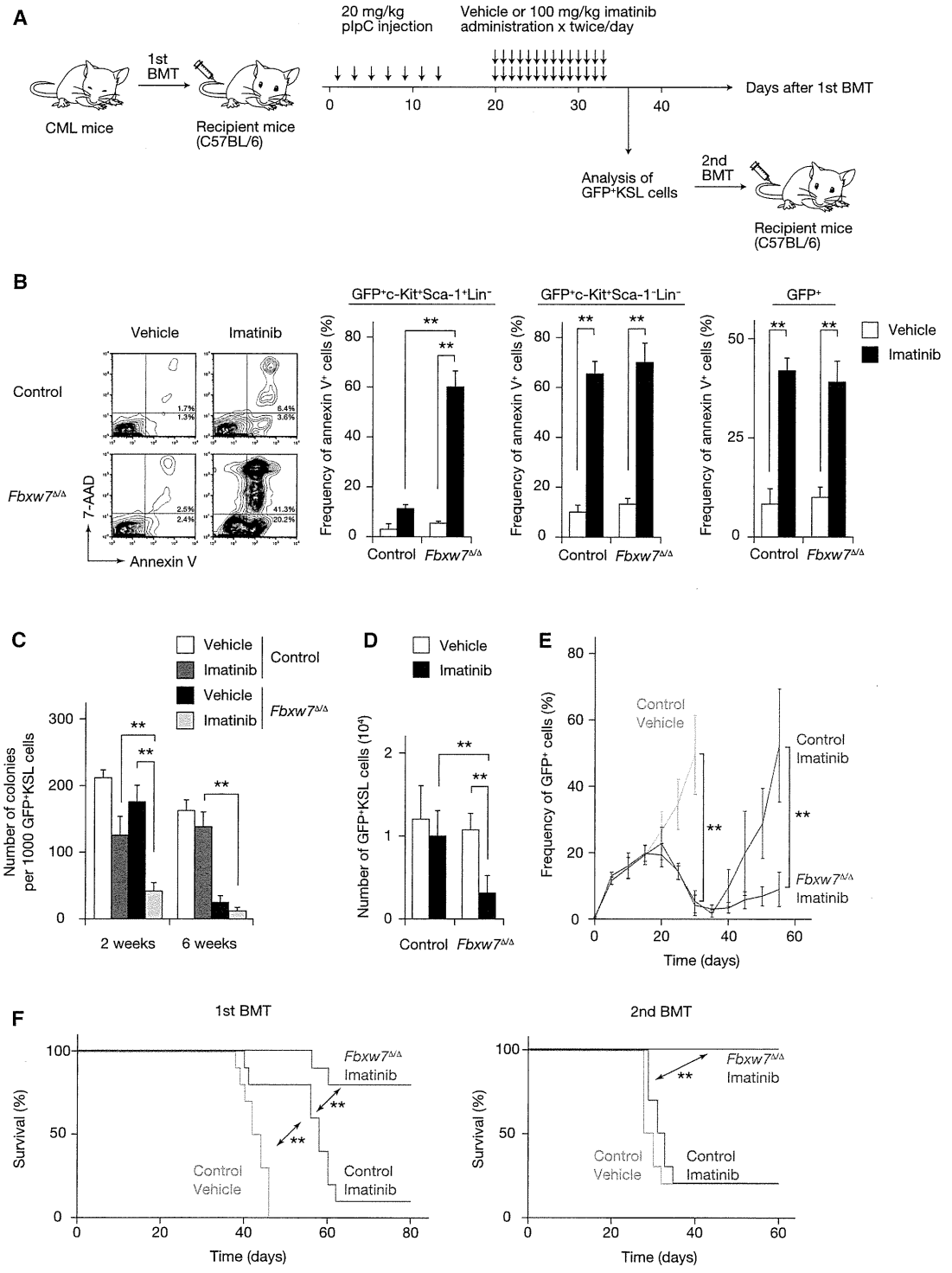

Figure 5. Combination Therapy with Fbxw7 Ablation and Imatinib Eliminates LICs

(A) Experimental strategy for combination therapy with Fbxw7 ablation and imatinib administration.

(B) Frequency of annexin V positivity among *Fbxw7*$^{\Delta/\Delta}$ or control cells of the indicated fractions isolated from recipients (n = 3) of the first BMT after treatment with imatinib or vehicle.

(C) Colony formation by *Fbxw7*$^{\Delta/\Delta}$ and control LICs cultured on OP-9 cells with imatinib or vehicle for 2 or 6 weeks (n = 3).

(D) Absolute number of GFP$^+$KSL cells in bone marrow from mice (n = 5) treated as in (A).

(E) Frequency of GFP$^+$ cells in peripheral blood from mice (n = 10) treated as in (A).

(F) Survival of recipients (n = 10) of the first and second BMT treated as in (A).

Data are means ± SD. **p < 0.01. See also Figure S4.

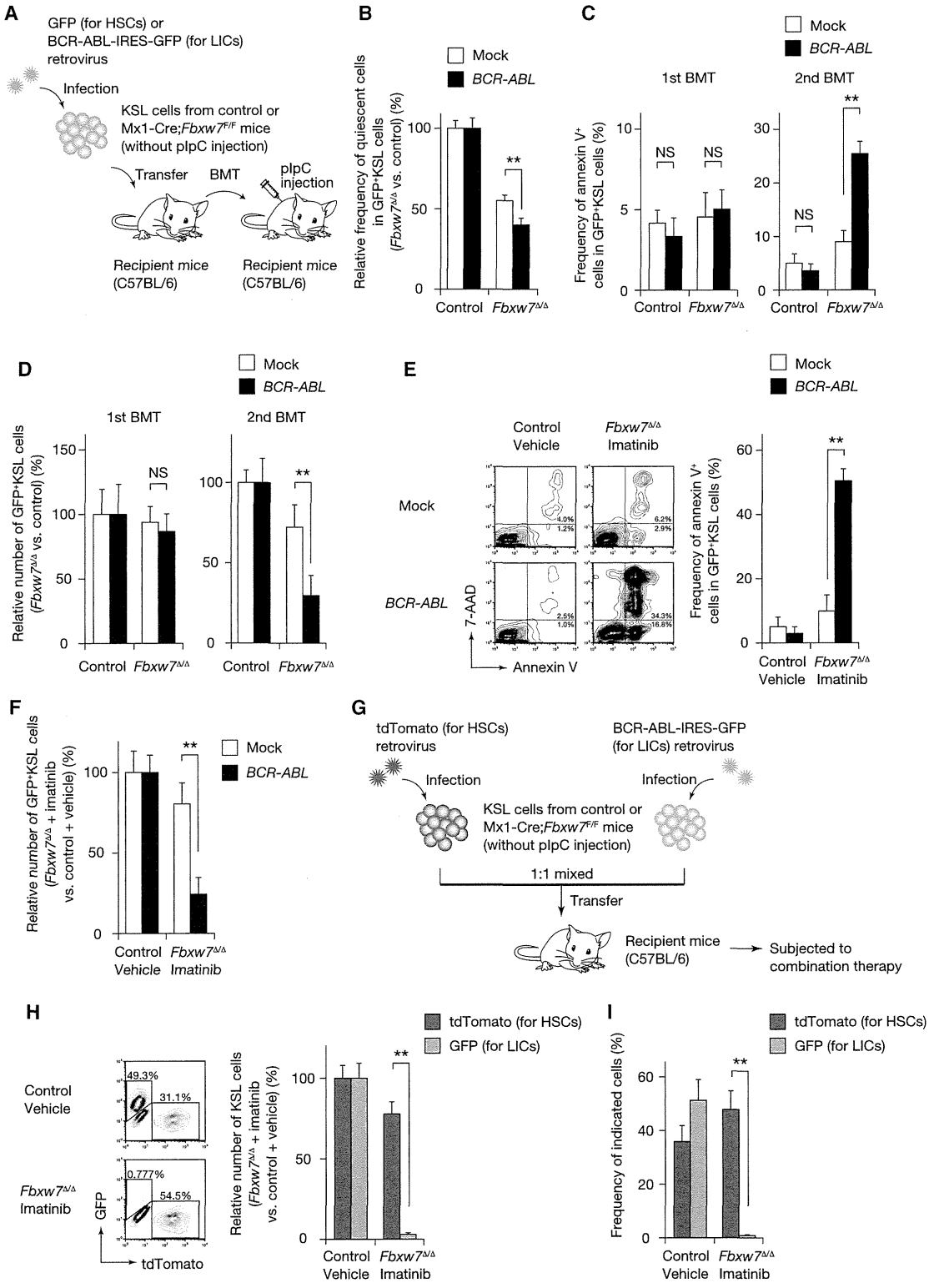

Figure 6. Fbxw7 Deficiency Affects LICs to a Greater Extent than It Does Normal HSCs

(A) Experimental strategy to compare the sensitivity of LICs to Fbxw7 deficiency with that of normal HSCs.

(B) The relative percentage of quiescent cells among GFP$^+$KSL cells for *Fbxw7*$^{\Delta/\Delta}$ cells compared with that for control cells infected with the corresponding vector was determined for recipients of the first BMT (n = 5).

(C) The frequency of annexin V$^+$ cells among GFP$^+$KSL cells for *Fbxw7*$^{\Delta/\Delta}$ cells compared with that for control cells infected with the corresponding vector was determined for recipients of the first and second BMTs (n = 3).

(legend continued on next page)

Fbxw7 ablation and imatinib administration between HSCs and LICs. The frequency of apoptosis among cells from recipient mice treated with this combination therapy was markedly greater for LICs than for HSCs (Figure 6E). Consistent with these results, the decrease in the number of stem cells was more prominent for LICs than for HSCs after combination therapy (Figure 6F).

Finally, to determine directly whether this combination therapy is able to eradicate LICs while preserving normal HSC function, we transplanted an equal number (1×10^4) of KSL cells infected with a retrovirus encoding the fluorescent marker tdTomato (to yield HSCs) and of KSL cells infected with the virus for BCR-ABL and GFP (to yield LICs) into the same recipient mice and then subjected the animals to combination therapy (Figure 6G). Flow cytometric analysis revealed that this regimen reduced the number of GFP^+KSL cells (LICs) to a greater extent than it did that of $tdTomato^+$KSL cells (HSCs) (Figure S5G). We then collected the same number (1×10^4) of $tdTomato^+$KSL cells and GFP^+KSL cells from these recipients and again transplanted them together into new recipients. Whereas Fbxw7-deficient $tdTomato^+$KSL cells (HSCs) persisted in these new recipients, almost all Fbxw7-deficient GFP^+KSL cells (LICs) were eradicated (Figure 6H). Furthermore, whereas $tdTomato^+$ cells (normal progeny of HSCs) were detected in the peripheral blood, virtually no GFP^+ cells (leukemic progeny of LICs) were detected (Figure 6I). Collectively, these observations thus reveal a difference in sensitivity to the combination therapy between HSCs and LICs, referred to as a "therapeutic window," and they thus provide a rationale for further development of this potential approach to the treatment of human leukemia.

Downregulation of Fbxw7 Is Effective for Eradication of Human LICs

To examine whether Fbxw7 ablation is indeed effective for eradication of human LICs in CML, we first measured the amount of Fbxw7 mRNA at various stages of the differentiation of bone marrow cells from patients in the chronic phase of CML. Similar to our findings with the mouse model of CML (Figure 1B), Fbxw7 mRNA was abundant in the LIC compartment ($CD34^+CD38^-Lin^-$ fraction), and its amount decreased markedly as the cells differentiated (Figure 7A). We next transfected bone marrow cells from such patients with small interfering RNAs (siRNAs) specific for Fbxw7 by electroporation, and we confirmed that almost all LICs were successfully transfected without induction of a substantial level of apoptosis by the procedure (Figure S6A) and that Fbxw7 mRNA was depleted efficiently (Figure 7B). Transfection with either of two independent such siRNAs resulted in a decrease in the proportion of quiescent cells in the LIC compartment (Figure 7C). Depletion of Fbxw7 in human LICs resulted in marked enhancement of the induction of apoptosis (Figure 7D) and the inhibition of colony formation (Figure 7E) by imatinib. Similar results were obtained with human LICs subjected to combination therapy with Fbxw7 depletion and Ara-C (Figures S6B and S6C).

Finally, we compared the sensitivity to Fbxw7 deficiency and combination therapy between human HSCs and LICs. We first measured the amount of Fbxw7 mRNA at various stages of the differentiation of bone marrow cells from healthy volunteers and found that Fbxw7 mRNA was abundant in HSCs and was downregulated during cell differentiation (Figure S6D). Depletion of Fbxw7 induced entry of human HSCs into the cell cycle (Figure S6E), and, as with mouse HSCs and LICs, this effect was greater in LICs than in HSCs (Figure 7F). In addition, induction of apoptosis and inhibition of colony formation by the combination of Fbxw7 depletion and imatinib treatment were more pronounced in LICs than in HSCs (Figures 7G and 7H; Figure S6F). Together, these results suggested that the sensitivity to combination therapy differs markedly between human HSCs and LICs, as was the case with mouse HSCs and LICs and that such therapy is a promising approach to the treatment of human CML.

DISCUSSION

With the use of a mouse model of CML, we have found that Fbxw7 has an indispensable role in maintenance of the quiescence as well as the stemness of LICs. Fbxw7-deficient LICs became exhausted with time and incapable of generating CML in transplanted animals. In contrast to LICs, leukemic progenitors proliferated rapidly, and their cell cycle status was not affected by Fbxw7 deficiency. The abundance of Fbxw7 mRNA was high in LICs and relatively low in leukemic progenitors, suggesting that Fbxw7 expression is regulated at the transcriptional level during leukemogenesis. The difference in cell cycle status between LICs and leukemic progenitors is therefore likely attributable, at least in part, to the difference in the abundance of Fbxw7 in these cells. Although the mechanisms responsible for regulation of Fbxw7 expression remain unknown, given that the HSC niche is thought to maintain HSCs in a quiescent state, it is possible that signals from the LIC niche may control Fbxw7 expression in LICs.

Our data also provide mechanistic insight into the maintenance of LIC quiescence by Fbxw7. We found that c-Myc accumulated in Fbxw7-deficient LICs, and either treatment with a c-Myc inhibitor or deletion of one allele of the c-Myc gene

(D) The relative number of GFP^+KSL cells among $Fbxw7^{\Delta/\Delta}$ cells compared with that for control cells infected with the corresponding vector was determined for recipients of the first and second BMTs (n = 5).
(E) The proportion of apoptotic cells among GFP^+KSL cells isolated from recipient mice harboring retrovirus-infected Mx1-Cre;$Fbxw7^{F/F}$ or control cells and injected with pIpC and then treated with imatinib or vehicle for 14 days was determined (n = 3).
(F) The number of GFP^+KSL cells in recipient mice processed as in (E) was determined relative to that in corresponding vehicle-treated recipients (n = 5).
(G) Experimental strategy to examine directly the difference in sensitivity to combination therapy between LICs and normal HSCs.
(H) An equal number (1×10^4) of $tdTomato^+$KSL cells and GFP^+KSL cells was collected from the recipients treated as in (G) and transplanted into new recipient mice together with 2×10^5 bone marrow cells from wild-type mice (second BMT). The relative numbers of $tdTomato^+$KSL cells and GFP^+KSL cells in the recipients (n = 5) of the second BMT were determined.
(I) The frequencies of $tdTomato^+$ cells and GFP^+ cells in peripheral blood from the recipients (n = 10) of the second BMT obtained as in (H) were determined.
Data are means ± SD. **$p < 0.01$; NS, not significant. See also Figure S5.

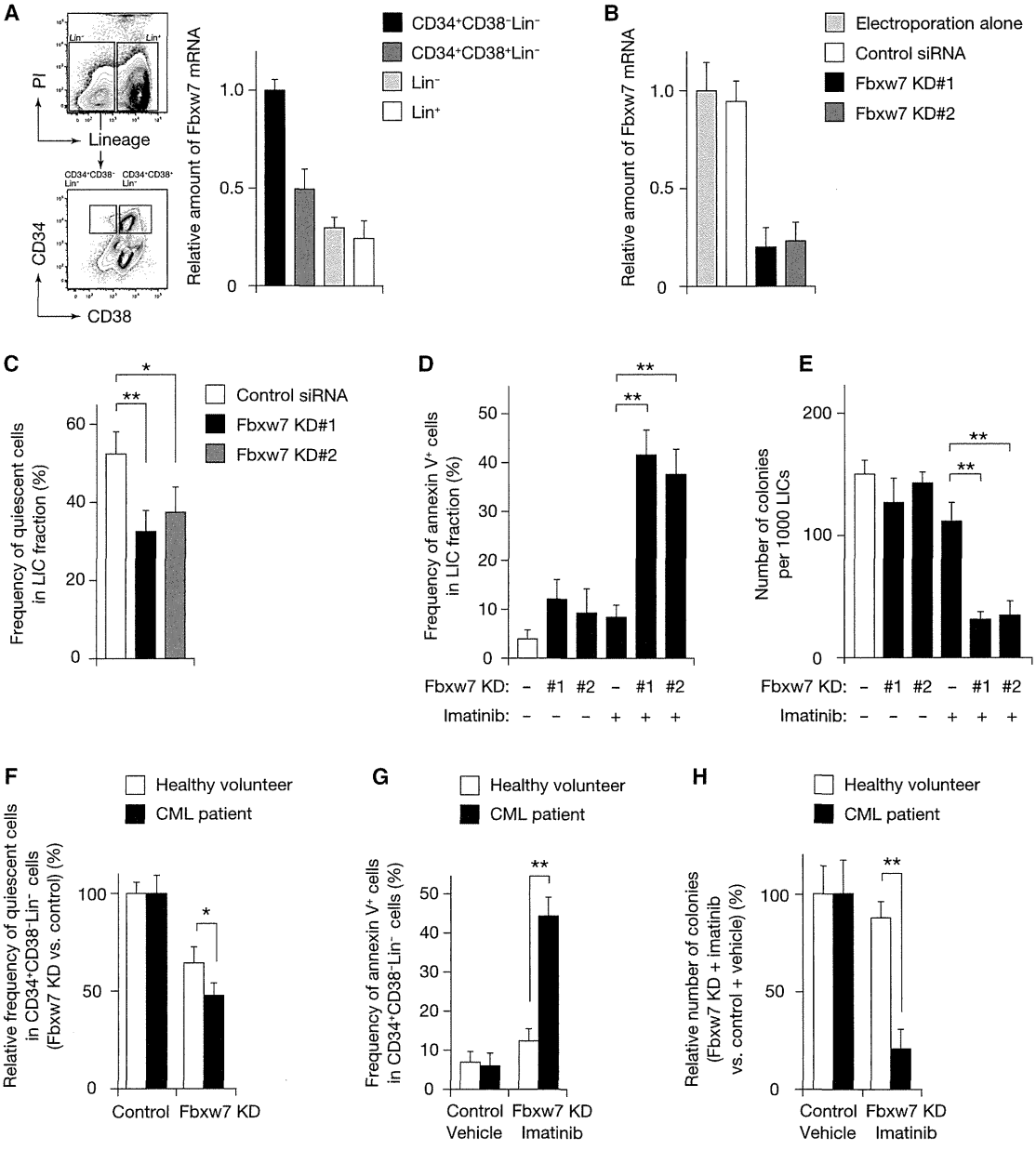

Figure 7. Combination Therapy with Fbxw7 Downregulation and Imatinib Is Effective for Eradication of Human LICs

(A) Bone marrow cells at various stages of differentiation from CML patients were fractionated by FACS and assayed for Fbxw7 mRNA by RT and real-time PCR analysis (n = 3).

(B) Bone marrow cells from patients with CML were transfected with a control siRNA or one of two independent Fbxw7 siRNAs (KD#1 or KD#2), after which the $CD34^+CD38^-Lin^-$ fraction was cultured on OP-9 cells for 3 days and then assayed for Fbxw7 mRNA (n = 3).

(C) Bone marrow cells from CML patients were transfected with Fbxw7 siRNAs, after which the $CD34^+CD38^-Lin^-$ fraction was sorted and cultured on OP-9 cells as in (B). The frequency of quiescent cells was then measured by flow cytometry (n = 3).

(D) Cells from CML patients were transfected, sorted, and cultured on OP-9 cells for 7 days. The cells were exposed (or not) to imatinib for the last 4 days of the culture, after which the proportion of apoptotic cells was determined by staining with annexin V (n = 3).

(E) Colony formation by human CML LICs transfected with Fbxw7 siRNAs and treated with imatinib as in (D) (n = 3).

(F) The relative frequencies of quiescent cells among human HSCs and LICs transfected with Fbxw7 or control siRNAs were determined as in (C) (n = 3).

(G) The frequency of annexin V^+ cells in human HSCs and LICs treated as in (D) (n = 3).

(H) The relative numbers of colonies formed by human HSCs and LICs transfected with Fbxw7 or control siRNAs and treated with vehicle or imatinib as in (D) were determined (n = 3).

Data are means ± SD. *$p < 0.05$; **$p < 0.01$. NS, not significant. See also Figure S6.

normalized the phenotype of these cells, including their cell cycle status and colony formation capacity. These results support the notion that c-Myc activation is responsible for cell cycle progression and the resulting exhaustion of Fbxw7-deficient LICs. Previous studies have indicated that an increase in metabolic growth signaling alone, including activation of the mTOR signaling pathway, is sufficient to drive quiescent HSCs into the proliferative state (Yilmaz et al., 2006). Given that mTOR is a candidate substrate of Fbxw7 (Mao et al., 2008), it was possible that increased mTOR activity might be responsible for the phenotype of Fbxw7-deficient LICs. However, we found that mTOR did not accumulate in Fbxw7-deficient LICs, and the mTOR signaling inhibitor rapamycin did not rescue the phenotype of these cells. We therefore conclude that mTOR activity is not related to the phenotype of Fbxw7-deficient LICs.

We also provide evidence that Fbxw7-deficient LICs are sensitive to anticancer drugs and that combination therapy with Fbxw7 ablation and such drugs is effective for LIC eradication, resulting in a survival advantage over treatment with anticancer drugs alone. Although the development of imatinib has substantially improved the prognosis of CML patients (Druker et al., 2001; Kantarjian et al., 2002), CML LICs are resistant to imatinib and residual LICs give rise to relapse after discontinuation of imatinib treatment (Mahon et al., 2010). Several mechanisms underlying resistance to imatinib have been proposed, including quiescence, BCR-ABL mutations such as T315I, and the lack of addiction to BCR-ABL in LICs (Corbin et al., 2011; Gorre et al., 2001; Holtz et al., 2007). Although more potent TKIs such as nilotinib and dasatinib have been developed, these drugs are also not able to overcome these mechanisms of TKI resistance in LICs (Copland et al., 2006; Jørgensen et al., 2007). We now show that combination therapy with Fbxw7 ablation and imatinib markedly reduced the rate of relapse after discontinuation of imatinib. We also obtained results suggesting that such combination therapy is effective for eradication of LICs in human CML.

Although our study suggests that inhibition of Fbxw7 might represent a promising therapeutic approach for CML patients, the application of Fbxw7 inhibition to the treatment of cancer warrants careful consideration. Given that Fbxw7 has been regarded as an oncosuppressor protein because it targets many proto-oncoproteins, growth promoters, and antiapoptotic molecules including cyclin E, c-Myc, Notch, c-Jun (Nakayama and Nakayama, 2006), mTOR (Mao et al., 2008), and Mcl-1 (Inuzuka et al., 2011; Wertz et al., 2011), suppression of Fbxw7 might induce carcinogenesis or promote cancer growth. Nevertheless, our experimental evidence indicates that the combination therapy with Fbxw7 ablation and anticancer drugs is effective for treatment of CML in a mouse model at the animal level as well as for eradication of human LICs.

Another concern about Fbxw7-targeted therapy is whether normal stem cells might be damaged. Fbxw7 also plays a pivotal role in HSC maintenance (Matsuoka et al., 2008; Thompson et al., 2008), and recent studies have shown that Fbxw7 is a key regulator of the viability of neural stem and progenitor cells (Hoeck et al., 2010; Matsumoto et al., 2011a). Although we found that LICs are more sensitive to Fbxw7 deficiency than are HSCs, suggesting that there is a therapeutic window in targeting Fbxw7 for therapy, it remains to be determined to what extent Fbxw7 inhibition might damage stem cells in other tissues. To minimize damage to normal stem cells, we propose that Fbxw7 inhibitors should be used for only a limited period. Our present study suggests that the difference in sensitivity to Fbxw7 inhibition between LICs and HSCs is attributable at least in part to the difference in the abundance of Fbxw7 or c-Myc in these cells and that such therapy may be expandable to other types of human cancer. Fbxw7 is therefore a promising target for the discovery of anticancer drugs with a broad spectrum of activity against many human cancers.

EXPERIMENTAL PROCEDURES

Mice

Generation of *Fbxw7*$^{F/F}$ mice was described previously (Onoyama et al., 2007). They were crossed with Mx1-Cre transgenic mice (kindly provided by K. Rajewsky) to generate Mx1-Cre;*Fbxw7*$^{F/F}$ mice, and Mx1-Cre;*Fbxw7*$^{+/+}$ mice were used as controls. *Fbxw7*$^{F/F}$ mice were also crossed with *c-Myc*$^{F/F}$ mice (kindly provided by I.M. de Alboran) or *p53*$^{-/-}$ mice (Taconic). All these mice were backcrossed with C57BL/6 mice for more than five generations. Expression of Cre recombinase in transplant recipients was induced by intraperitoneal injection of pIpC (Merck) at a dose of 20 mg per kilogram of body mass on 7 alternate days. C57BL/6 mice were obtained from The Jackson Laboratory and were used as recipients. All mouse experiments were approved by the Animal Ethics Committee of Kyushu University. For some experiments, mice were injected intraperitoneally with Ara-C (Sigma) at a dose of 150 mg/kg. Imatinib (Novartis) was administered by oral gavage twice a day at a dose of 100 mg/kg.

Generation of CML Model

Immature c-Kit$^+$Sca-1$^+$Lin$^-$ hematopoietic cells (KSL cells) were isolated by fluorescence-activated cell sorting (FACS) from bone marrow of Mx1-Cre;*Fbxw7*$^{F/F}$ and Mx1-Cre;*Fbxw7*$^{+/+}$ mice and were cultured in serum-free S-Clone SF-O3 medium (Sanko Junyaku) supplemented with mouse stem cell factor (Wako) at 100 ng/ml as well as human thrombopoietin (PeproTech) at 100 ng/ml. For generation of the CML mouse model, the KSL cells were infected for 2 days with a retrovirus harboring the MSCV-BCR-ABL-IRES-GFP construct (see Supplemental Experimental Procedures) with the use of CombiMag (OZ Biosciences). GFP$^+$ cells (2×10^4) were then isolated by FACS and were injected intravenously into lethally irradiated (9.5 Gy) C57BL/6 mice together with 2×10^5 bone marrow cells from C57BL/6 mice. The efficiency of gene transduction as evaluated on the basis of GFP expression was 30 to 40% in all experiments. When the number of white blood cells had increased to >20,000 /μl, we collected 2×10^4 GFP$^+$KSL cells from the recipient mice and transferred them to new recipients together with 2×10^5 bone marrow cells from C57BL/6 mice (first BMT). These new recipients were injected with pIpC beginning the day after BMT as described earlier. For serial transplantation, 1×10^4 or 2×10^4 GFP$^+$KSL cells were collected from recipient mice 3 weeks after the first BMT and were transplanted into other recipient mice together with 2×10^5 bone marrow cells from C57BL/6 mice (second BMT).

Colony Formation Assays

Colony formation by mouse cells was examined with the use of Methocult medium (MethoCult GF M3434, StemCell Technologies). Control and *Fbxw7*$^{\Delta/\Delta}$ GFP$^+$KSL cells (1×10^3) were collected from recipients of the first BMT and then cultured under hypoxic (5% O_2) conditions with OP-9 stromal cells (Kodama et al., 1994) (RIKEN Cell Bank) for 2 or 6 weeks in six-well dishes containing α–minimum essential medium (Sigma) supplemented with 12.5% fetal bovine serum (Invitrogen), 12.5% horse serum (Invitrogen), and 1 nM dexamethasone (Wako). The cells (2×10^4) were then collected and transferred to Methocult medium. Colonies were scored 1 week after plating for determination of the number of colonies per 1000 GFP$^+$KSL cells. For some experiments, 100 μM 10058-F4 (Merck), 10 μM DAPT (Merck), 25 nM rapamycin (Cell Signaling Technology), 10 μM PFTα (Merck), 100 nM Ara-C, or 5 μM imatinib was added to the culture medium.

Analysis of Primary Human CML Samples

Viable bone marrow mononuclear cells from treatment-naive patients in the chronic phase of CML and from healthy volunteers who had given informed consent were obtained from AllCells. The use of these purchased samples was considered exempt by the Ethics Committee of Kyushu University. To examine the role of Fbxw7 in the maintenance of LICs for human CML and normal HSCs, we transfected bone marrow mononuclear cells with 300 nM Fbxw7 siRNAs (Stealth Select RNAi siRNA, Invitrogen) by electroporation with the use of an Amaxa Nucleofector II device (Lonza) according to the recommended protocol. The transfected cells were then stained with antibodies to human CD34 (8G12), CD38 (HIT2), CD3 (SK7), CD16 (3G8), CD19 (SJ25C1), CD20 (L27), CD14 (MϕP9), and CD56 (NCAM16.2) (BD Biosciences). CD3, CD16, CD19, CD20, CD14, and CD56 were used as lineage markers. $CD34^+CD38^-Lin^-$ cells (1×10^3) were purified by FACS and cocultured with OP-9 cells for 7 days. For some experiments, 100 nM Ara-C or 5 μM imatinib was added to the cultures for Days 3 to 7. The human cells were then assayed for apoptosis (see Supplemental Experimental Procedures) or for colony formation; for the latter assay, the cells were transferred to Methocult medium (MethoCult GF H4435, StemCell Technologies), and the number of colonies was counted 1 week after plating.

Statistical Analysis

Quantitative data are presented as means ± SD and were analyzed by Student's t test, with the exception that survival curves were analyzed by the log-rank nonparametric test. A p value of < 0.05 was considered statistically significant.

Other Experimental Procedures

Flow cytometry, preparation of recombinant retroviruses, cell cycle analysis, detection of apoptosis, RT and real-time PCR analysis, and immunoblot analysis are described in Supplemental Experimental Procedures.

SUPPLEMENTAL INFORMATION

Supplemental Information includes six figures and Supplemental Experimental Procedures and can be found in this article online at http://dx.doi.org/10.1016/j.ccr.2013.01.026.

ACKNOWLEDGMENTS

We thank K. Rajewsky for Mx1-Cre transgenic mice, I.M. de Alboran for *c-Myc*$^{F/F}$ mice, H. Honda for BCR-ABL cDNA, and T. Kitamura for Plat-E retroviral packaging cells.

Received: June 29, 2011
Revised: April 25, 2012
Accepted: January 22, 2013
Published: March 18, 2013

REFERENCES

Clevers, H. (2011). The cancer stem cell: premises, promises and challenges. Nat. Med. *17*, 313–319.

Copland, M., Hamilton, A., Elrick, L.J., Baird, J.W., Allan, E.K., Jordanides, N., Barow, M., Mountford, J.C., and Holyoake, T.L. (2006). Dasatinib (BMS-354825) targets an earlier progenitor population than imatinib in primary CML but does not eliminate the quiescent fraction. Blood *107*, 4532–4539.

Corbin, A.S., Agarwal, A., Loriaux, M., Cortes, J., Deininger, M.W., and Druker, B.J. (2011). Human chronic myeloid leukemia stem cells are insensitive to imatinib despite inhibition of BCR-ABL activity. J. Clin. Invest. *121*, 396–409.

de Klein, A., van Kessel, A.G., Grosveld, G., Bartram, C.R., Hagemeijer, A., Bootsma, D., Spurr, N.K., Heisterkamp, N., Groffen, J., and Stephenson, J.R. (1982). A cellular oncogene is translocated to the Philadelphia chromosome in chronic myelocytic leukaemia. Nature *300*, 765–767.

Deininger, M.W., Goldman, J.M., and Melo, J.V. (2000). The molecular biology of chronic myeloid leukemia. Blood *96*, 3343–3356.

Druker, B.J., Talpaz, M., Resta, D.J., Peng, B., Buchdunger, E., Ford, J.M., Lydon, N.B., Kantarjian, H., Capdeville, R., Ohno-Jones, S., and Sawyers, C.L. (2001). Efficacy and safety of a specific inhibitor of the BCR-ABL tyrosine kinase in chronic myeloid leukemia. N. Engl. J. Med. *344*, 1031–1037.

Essers, M.A., Offner, S., Blanco-Bose, W.E., Waibler, Z., Kalinke, U., Duchosal, M.A., and Trumpp, A. (2009). IFNalpha activates dormant haematopoietic stem cells in vivo. Nature *458*, 904–908.

Follis, A.V., Hammoudeh, D.I., Daab, A.T., and Metallo, S.J. (2009). Small-molecule perturbation of competing interactions between c-Myc and Max. Bioorg. Med. Chem. Lett. *19*, 807–810.

Gorre, M.E., Mohammed, M., Ellwood, K., Hsu, N., Paquette, R., Rao, P.N., and Sawyers, C.L. (2001). Clinical resistance to STI-571 cancer therapy caused by BCR-ABL gene mutation or amplification. Science *293*, 876–880.

Hoeck, J.D., Jandke, A., Blake, S.M., Nye, E., Spencer-Dene, B., Brandner, S., and Behrens, A. (2010). Fbw7 controls neural stem cell differentiation and progenitor apoptosis via Notch and c-Jun. Nat. Neurosci. *13*, 1365–1372.

Holtz, M., Forman, S.J., and Bhatia, R. (2007). Growth factor stimulation reduces residual quiescent chronic myelogenous leukemia progenitors remaining after imatinib treatment. Cancer Res. *67*, 1113–1120.

Huntly, B.J., and Gilliland, D.G. (2005). Leukaemia stem cells and the evolution of cancer-stem-cell research. Nat. Rev. Cancer *5*, 311–321.

Inuzuka, H., Shaik, S., Onoyama, I., Gao, D., Tseng, A., Maser, R.S., Zhai, B., Wan, L., Gutierrez, A., Lau, A.W., et al. (2011). $SCF^{(FBW7)}$ regulates cellular apoptosis by targeting MCL1 for ubiquitylation and destruction. Nature *471*, 104–109.

Ito, K., Bernardi, R., Morotti, A., Matsuoka, S., Saglio, G., Ikeda, Y., Rosenblatt, J., Avigan, D.E., Teruya-Feldstein, J., and Pandolfi, P.P. (2008). PML targeting eradicates quiescent leukaemia-initiating cells. Nature *453*, 1072–1078.

Jørgensen, H.G., Allan, E.K., Jordanides, N.E., Mountford, J.C., and Holyoake, T.L. (2007). Nilotinib exerts equipotent antiproliferative effects to imatinib and does not induce apoptosis in $CD34^+$ CML cells. Blood *109*, 4016–4019.

Kantarjian, H., Sawyers, C., Hochhaus, A., Guilhot, F., Schiffer, C., Gambacorti-Passerini, C., Niederwieser, D., Resta, D., Capdeville, R., Zoellner, U., et al.; International STI571 CML Study Group. (2002). Hematologic and cytogenetic responses to imatinib mesylate in chronic myelogenous leukemia. N. Engl. J. Med. *346*, 645–652.

Kodama, H., Nose, M., Niida, S., Nishikawa, S., and Nishikawa, S. (1994). Involvement of the c-kit receptor in the adhesion of hematopoietic stem cells to stromal cells. Exp. Hematol. *22*, 979–984.

Komarov, P.G., Komarova, E.A., Kondratov, R.V., Christov-Tselkov, K., Coon, J.S., Chernov, M.V., and Gudkov, A.V. (1999). A chemical inhibitor of p53 that protects mice from the side effects of cancer therapy. Science *285*, 1733–1737.

Lapidot, T., Sirard, C., Vormoor, J., Murdoch, B., Hoang, T., Caceres-Cortes, J., Minden, M., Paterson, B., Caligiuri, M.A., and Dick, J.E. (1994). A cell initiating human acute myeloid leukaemia after transplantation into SCID mice. Nature *367*, 645–648.

Laurenti, E., Wilson, A., and Trumpp, A. (2009). Myc's other life: stem cells and beyond. Curr. Opin. Cell Biol. *21*, 844–854.

Mahon, F.X., Réa, D., Guilhot, J., Guilhot, F., Huguet, F., Nicolini, F., Legros, L., Charbonnier, A., Guerci, A., Varet, B., et al.; Intergroupe Français des Leucémies Myéloïdes Chroniques. (2010). Discontinuation of imatinib in patients with chronic myeloid leukaemia who have maintained complete molecular remission for at least 2 years: the prospective, multicentre Stop Imatinib (STIM) trial. Lancet Oncol. *11*, 1029–1035.

Mao, J.H., Kim, I.J., Wu, D., Climent, J., Kang, H.C., DelRosario, R., and Balmain, A. (2008). FBXW7 targets mTOR for degradation and cooperates with PTEN in tumor suppression. Science *321*, 1499–1502.

Matsumoto, A., Onoyama, I., Sunabori, T., Kageyama, R., Okano, H., and Nakayama, K.I. (2011a). Fbxw7-dependent degradation of Notch is required for control of "stemness" and neuronal-glial differentiation in neural stem cells. J. Biol. Chem. *286*, 13754–13764.

Matsumoto, A., Takeishi, S., Kanie, T., Susaki, E., Onoyama, I., Tateishi, Y., Nakayama, K., and Nakayama, K.I. (2011b). p57 is required for quiescence and maintenance of adult hematopoietic stem cells. Cell Stem Cell *9*, 262–271.

Matsuoka, S., Oike, Y., Onoyama, I., Iwama, A., Arai, F., Takubo, K., Mashimo, Y., Oguro, H., Nitta, E., Ito, K., et al. (2008). Fbxw7 acts as a critical fail-safe against premature loss of hematopoietic stem cells and development of T-ALL. Genes Dev. *22*, 986–991.

Naka, K., Hoshii, T., Muraguchi, T., Tadokoro, Y., Ooshio, T., Kondo, Y., Nakao, S., Motoyama, N., and Hirao, A. (2010). TGF-β-FOXO signalling maintains leukaemia-initiating cells in chronic myeloid leukaemia. Nature *463*, 676–680.

Nakayama, K.I., and Nakayama, K. (2006). Ubiquitin ligases: cell-cycle control and cancer. Nat. Rev. Cancer *6*, 369–381.

Onoyama, I., Tsunematsu, R., Matsumoto, A., Kimura, T., de Alborán, I.M., Nakayama, K., and Nakayama, K.I. (2007). Conditional inactivation of Fbxw7 impairs cell-cycle exit during T cell differentiation and results in lymphomatogenesis. J. Exp. Med. *204*, 2875–2888.

Pear, W.S., Miller, J.P., Xu, L., Pui, J.C., Soffer, B., Quackenbush, R.C., Pendergast, A.M., Bronson, R., Aster, J.C., Scott, M.L., and Baltimore, D. (1998). Efficient and rapid induction of a chronic myelogenous leukemia-like myeloproliferative disease in mice receiving P210 bcr/abl-transduced bone marrow. Blood *92*, 3780–3792.

Reavie, L., Della Gatta, G., Crusio, K., Aranda-Orgilles, B., Buckley, S.M., Thompson, B., Lee, E., Gao, J., Bredemeyer, A.L., Helmink, B.A., et al. (2010). Regulation of hematopoietic stem cell differentiation by a single ubiquitin ligase-substrate complex. Nat. Immunol. *11*, 207–215.

Rowley, J.D. (1973). Letter: A new consistent chromosomal abnormality in chronic myelogenous leukaemia identified by quinacrine fluorescence and Giemsa staining. Nature *243*, 290–293.

Thompson, B.J., Jankovic, V., Gao, J., Buonamici, S., Vest, A., Lee, J.M., Zavadil, J., Nimer, S.D., and Aifantis, I. (2008). Control of hematopoietic stem cell quiescence by the E3 ubiquitin ligase Fbw7. J. Exp. Med. *205*, 1395–1408.

Wertz, I.E., Kusam, S., Lam, C., Okamoto, T., Sandoval, W., Anderson, D.J., Helgason, E., Ernst, J.A., Eby, M., Liu, J., et al. (2011). Sensitivity to antitubulin chemotherapeutics is regulated by MCL1 and FBW7. Nature *471*, 110–114.

Yamazaki, S., Ema, H., Karlsson, G., Yamaguchi, T., Miyoshi, H., Shioda, S., Taketo, M.M., Karlsson, S., Iwama, A., and Nakauchi, H. (2011). Nonmyelinating Schwann cells maintain hematopoietic stem cell hibernation in the bone marrow niche. Cell *147*, 1146–1158.

Yilmaz, O.H., Valdez, R., Theisen, B.K., Guo, W., Ferguson, D.O., Wu, H., and Morrison, S.J. (2006). Pten dependence distinguishes haematopoietic stem cells from leukaemia-initiating cells. Nature *441*, 475–482.

Zhang, X., and Ren, R. (1998). Bcr-Abl efficiently induces a myeloproliferative disease and production of excess interleukin-3 and granulocyte-macrophage colony-stimulating factor in mice: a novel model for chronic myelogenous leukemia. Blood *92*, 3829–3840.

Zhao, C., Blum, J., Chen, A., Kwon, H.Y., Jung, S.H., Cook, J.M., Lagoo, A., and Reya, T. (2007). Loss of β-catenin impairs the renewal of normal and CML stem cells in vivo. Cancer Cell *12*, 528–541.

Cell

FBXL21 Regulates Oscillation of the Circadian Clock through Ubiquitination and Stabilization of Cryptochromes

Arisa Hirano,[1] Kanae Yumimoto,[2] Ryosuke Tsunematsu,[2] Masaki Matsumoto,[2] Masaaki Oyama,[3] Hiroko Kozuka-Hata,[3] Tomoki Nakagawa,[1] Darin Lanjakornsiripan,[1] Keiichi I. Nakayama,[2,*] and Yoshitaka Fukada[1,*]

[1]Department of Biophysics and Biochemistry, Graduate School of Science, The University of Tokyo, 7-3-1 Hongo, Bunkyo-ku, Tokyo 113-0033, Japan

[2]Department of Molecular and Cellular Biology, Medical Institute of Bioregulation, Kyushu University, 3-1-1 Maidashi, Higashi-ku, Fukuoka, Fukuoka 812-8582, Japan

[3]Medical Proteomics Laboratory, Institute of Medical Science,The University of Tokyo, 4-6-1 Shirokanedai, Minato-ku, Tokyo 108-8639, Japan

*Correspondence: nakayak1@bioreg.kyushu-u.ac.jp (K.I.N.), sfukada@mail.ecc.u-tokyo.ac.jp (Y.F.)

http://dx.doi.org/10.1016/j.cell.2013.01.054

SUMMARY

In the mammalian circadian clockwork, CRY1 and CRY2 repressor proteins are regulated by posttranslational modifications for temporally coordinated transcription of clock genes. Previous studies revealed that FBXL3, an F-box-type E3 ligase, ubiquitinates CRYs and mediates their degradation. Here, we found that FBXL21 also ubiquitinates CRYs but counteracts FBXL3. *Fbxl21*$^{-/-}$ mice exhibited normal periodicity of wheel-running rhythms with compromised organization of daily activities, while an extremely long-period phenotype of *Fbxl3*$^{-/-}$ mice was attenuated in *Fbxl3/Fbxl21* double-knockout mice. The double knockout destabilized the behavioral rhythms progressively and sometimes elicited arrhythmicity. Surprisingly, FBXL21 stabilized CRYs and antagonized the destabilizing action by FBXL3. Predominantly cytosolic distribution of FBXL21 contrasts with nuclear localization of FBXL3. These results emphasize the physiological importance of antagonizing actions between FBXL21 and FBXL3 on CRYs, and their combined actions at different subcellular locations stabilize oscillation of the circadian clock.

INTRODUCTION

Circadian rhythms with a period of approximately 24 hr are generated by an internal timekeeping mechanism referred to as the circadian clock (Takahashi, 1995, Dunlap, 1999). In mammals, the central circadian pacemaker in the hypothalamic suprachiasmatic nucleus (SCN) governs behavioral rhythms and coordinates peripheral clocks located in a variety of tissues (Schibler and Sassone-Corsi, 2002; Hastings et al., 2003). The mammalian circadian clocks are driven by a transcription-translation-based negative feedback loop. In the clockwork, CLOCK-BMAL1 heterodimers activate transcription of PERIODs (PER1-3) and CRYPTOCHROMEs (CRY1 and CRY2) through binding to E-box enhancer-elements (Gekakis et al., 1998; Bunger et al., 2000). Translated PER and CRY proteins associate with each other, translocate into the nucleus, and repress their own transcription through interaction with CLOCK-BMAL1 (Kume et al., 1999; Shearman et al., 2000). Among the clock proteins, CRY1 and CRY2 act as key players in the mammalian clockwork through their strong repressive activities on CLOCK-BMAL1-dependent transcription (Kume et al., 1999; van der Horst et al., 1999).

In addition to the transcriptional regulation, posttranslational modifications of clock proteins have critical roles for the circadian oscillation of the molecular clock (Toh et al., 2001; Gallego and Virshup, 2007; Nolan and Parsons, 2009; Reischl and Kramer, 2011). We previously reported a posttranslational mechanism regulating the stability of CRY2 protein. CRY2 is phosphorylated at Ser557 in a circadian manner in the mouse SCN and liver (Harada et al., 2005; Kurabayashi et al., 2006). The priming phosphorylation of CRY2 at Ser557 by DYRK1A allows subsequent phosphorylation at Ser553 by GSK-3β, and the two-step phosphorylation at the two neighboring Ser residues of CRY2 leads to its proteasomal degradation (Kurabayashi et al., 2010). On the other hand, CRY1 and CRY2 are ubiquitinated by the Skp1-Cul1-FBXL3 (SCF^{FBXL3}) ubiquitin ligase complex (Busino et al., 2007), and the interaction of CRYs with FBXL3, an F-box protein, is promoted by AMP-activated protein kinase (AMPK)-mediated phosphorylation of CRYs (Lamia et al., 2009). FBXL3-mediated ubiquitination of CRYs leads to their proteasomal degradation, and two point mutations in mouse *Fbxl3*, i.e., *After-hour* (*Afh*) and *Overtime* (*Ovtm*), each cause remarkable lengthening of the free-running period of the mouse behavioral rhythms (Siepka et al., 2007; Godinho et al., 2007). However, CRY2-FBXL3 interaction and FBXL3-mediated CRY2 degradation do not require Ser557/Ser553 phosphorylation of CRY2 (Kurabayashi et al., 2010). Thus, CRY proteins are subject

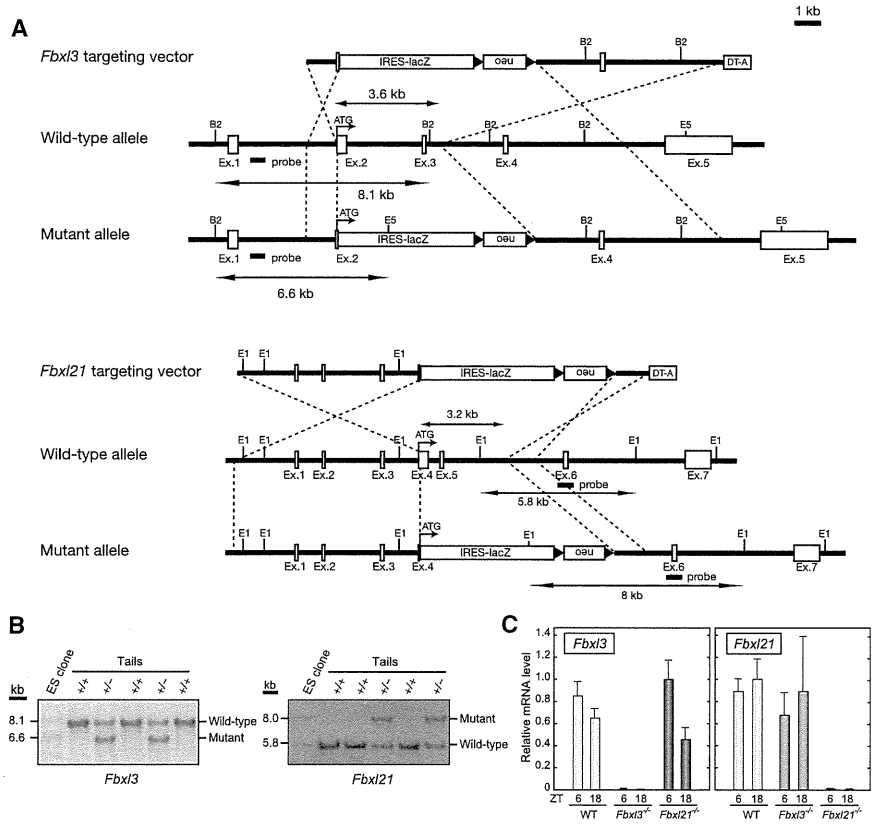

Figure 1. Generation of *Fbxl3* and *Fbxl21* Knockout Mice

(A) Targeting vectors for generation of *Fbxl3* knockout mice (*Fbxl3*$^{-/-}$) and *Fbxl21* knockout mice (*Fbxl21*$^{-/-}$).

(B) Southern blotting analysis of genomic DNA from tails of mice with the indicated genotypes for *Fbxl3* (left) or *Fbxl21* (right). The DNA was digested with BglII and EcoRV for *Fbxl3* or with EcoRI for *Fbxl21* genotyping. Hybridized probes are indicated in (A).

(C) *Fbxl3* (left) or *Fbxl21* (right) mRNA levels in the mouse liver quantified by real-time PCR. Data are means + SEM (n = 3) for wild-type and *Fbxl21*$^{-/-}$ mice and means + SD (n = 2) for *Fbxl3*$^{-/-}$ mice.

to degradation through at least two distinct pathways, postulating the involvement of another E3 ligase in the phosphorylation-dependent degradation of CRY2. Hence, we focused our attention on FBXL21, which is most similar in sequence to FBXL3 (84% amino acid sequence identity) among the F-box-type E3 ubiquitin ligase family (Jin et al., 2004; Dardente et al., 2008). Despite the similarity between these FBXL proteins, the physiological role of FBXL21 in the circadian clockwork remains to be elucidated (Dardente et al., 2008).

In this study, we show that FBXL21 ubiquitinates CRYs and that, surprisingly, FBXL21 stabilizes CRYs. FBXL21 localizes predominantly in the cytosol, whereas FBXL3 is present in the nucleus. Hence, the function and cellular distribution of FBXL21 form a sharp contrast with those of FBXL3 responsible for CRY protein degradation. The double knockout of *Fbxl3* and *Fbxl21* alleviated the circadian period-lengthening phenotype of *Fbxl3* knockout mice, further supporting their antagonizing actions on CRYs. Importantly, the double knockout destabilized the central clock in the SCN and progressively perturbed rhythmicity of the circadian behaviors in constant darkness. The antagonizing actions of *Fbxl3* and *Fbxl21* on CRY proteins have a critical role for robust oscillation of the mammalian circadian clock.

RESULTS

Generation of *Fbxl3* and *Fbxl21* Knockout Mice

Afh and *Ovtm* are two point-mutant alleles of *Fbxl3* (Siepka et al., 2007; Godinho et al., 2007). To evaluate the in vivo roles of *Fbxl3* and its closely related paralog, *Fbxl21*, we generated knockout mice lacking *Fbxl3* and/or *Fbxl21*. We created targeting vectors, in which IRES-*lacZ* and *neo* cassettes were introduced into the coding region of *Fbxl3* or *Fbxl21* gene (Figure 1A). Germline transmission of the mutant allele was confirmed by Southern blot analysis (Figure 1B). Heterozygous offspring crossed with C57BL/6 mice for at least seven generations were intercrossed to produce *Fbxl3* or *Fbxl21* knockout mice. In both cases, the genotypic distribution of the offspring followed Mendelian inheritance, and all the knockout mice used in the present study were normal in appearance. The messenger RNA (mRNA) levels of *Fbxl3* and *Fbxl21* in the liver of wild-type, *Fbxl3*$^{-/-}$, and *Fbxl21*$^{-/-}$ mice were analyzed by real-time PCR. *Fbxl3* or *Fbxl21* deficiency had no significant effect on the expression levels of *Fbxl21* or *Fbxl3*, respectively, when compared to their mRNA levels in the wild-type liver (Figure 1C).

Fbxl3 and *Fbxl21* Are Essential for Normal Behavioral Rhythms

We examined the effects of deficiencies of *Fbxl3* and/or *Fbxl21* on the behavioral rhythms of mice by monitoring their wheel-running activities (Figures 2A–2D). *Fbxl3* null mice apparently entrained to the 12L:12D (LD) cycle, although the onset of active phase was abnormally delayed from the light-to-dark transition (Figure 2E; Table S1 available online). In constant darkness (DD), *Fbxl3*-deficient mice showed rhythmic activities with a free-running period (τ_{DD}) of 27.74 ± 0.20 hr (Figure 1F and Table S1), which was significantly longer than that of their wild-type littermates (τ_{DD}: 23.77 ± 0.06 hr). Such an extremely long period in *Fbxl3*-deficient mice probably caused the delay of activity onset in LD. When transferred from DD to LD, 5 out of 14 *Fbxl3* knockout mice failed to entrain to the 24 hr cycle (Table S1) and apparently free ran as they did in DD (Figure 2C), a phenotype also observed in *Afh* mutant mice (Godinho et al., 2007). The circadian phenotype of *Fbxl3*-deficient mice (τ_{DD}: 27.74 ± 0.20 hr) was more severe than those of *Fbxl3*$^{Afh/Afh}$ (τ_{DD}: 26.5 hr, Godinho et al., 2007) and *Fbxl3*$^{Ovtm/Ovtm}$ (τ_{DD}: 26.21 hr,

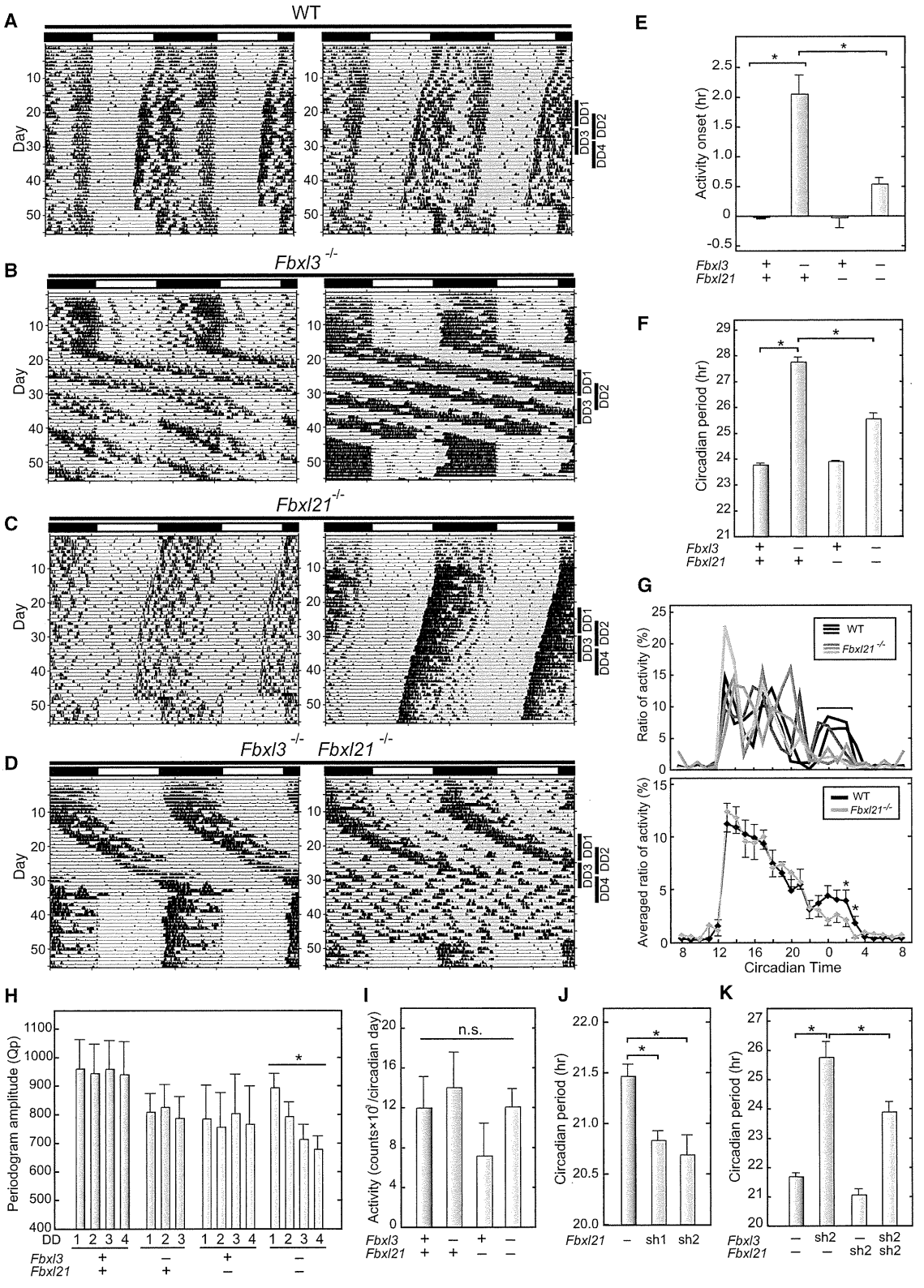

Figure 2. Wheel-Running Activity of *Fbxl3* and *Fbxl21* Knockout Mice

(A–D) Representative actograms of the wheel-running activities of wild-type (A), *Fbxl3*$^{-/-}$ *Fbxl21*$^{+/+}$ (B), *Fbxl3*$^{+/+}$ *Fbxl21*$^{-/-}$ (C), and *Fbxl3*$^{-/-}$ *Fbxl21*$^{-/-}$ (D). Mice were entrained to LD cycle for at least 5 weeks, transferred to DD, and then transferred to LD again.

(legend continued on next page)

Siepka et al., 2007). Thus, *Fbxl3* plays an important role in the regulation of the oscillation speed of the circadian clock in mice.

On the other hand, *Fbxl21*-deficient mice exhibited no significant difference from their wild-type littermates in both the free-running period in DD (Figure 2F) and activity onset in LD (Figure 2E). However, an alteration in the daily activities was obviously observed in *Fbxl21* null mice: During the active period, wild-type mice showed two peaks of activity bouts at early and late night, the latter of which was eliminated in *Fbxl21*-deficient mice (Figure 2G). This observation implies an involvement of *Fbxl21* in the SCN clock regulating temporal organization of the daily activities.

The strong phenotype of *Fbxl3* null mice in behavioral rhythm (τ_{DD}: 27.74 ± 0.20 hr) was significantly attenuated in *Fbxl3/Fbxl21* double-knockout mice (Figures 2D and 2F; τ_{DD}: 25.59 ± 0.15 hr). The abnormal delay of the activity onset observed in *Fbxl3* knockout mice in LD was also alleviated in the double-knockout mice (Figure 2E). However, we found that the double-knockout mice exhibited unstable behavioral rhythms in DD, although all of *Fbxl3* single-knockout mice showed rhythmic behaviors in DD: three out of ten *Fbxl3/Fbxl21* knockout mice were initially rhythmic but became arrhythmic within a few weeks after they were transferred to DD (Figure 2D, right panel; Table S1). We estimated the robustness of the behavioral rhythms for all the mice by the chi square periodogram procedure, where robustness is expressed as the Qp statistic reflecting the strength or regularity of a rhythm (Sokolove and Bushell, 1978). The double-knockout mice showed a progressive decline in Qp statistic during days 9–28 in DD (Figure 2H). This vulnerability was not observed in *Fbxl3* and *Fbxl21* single-knockout mice (Figure 2H; Table S1). It is therefore evident that *Fbxl3/Fbxl21* double deficiency destabilized the circadian oscillator in the SCN with no significant effect on the daily levels of wheel-running activity (Figure 2I). We conclude that the combined actions of *Fbxl21* and *Fbxl3* play a key role in the maintenance of both the speed and the robustness of the circadian clock oscillation.

Fbxl21 Regulates the Oscillation Speed of Cellular Clocks

A role of *Fbxl21* in the cellular clock was investigated in NIH 3T3 cells. To monitor the cellular rhythms, we introduced a luciferase reporter under the regulation of *Bmal1* promoter into the cultured cells by transient transfection. Silencing of *Fbxl21* was performed by cotransfection of an expression plasmid of small hairpin RNA (shRNA) sh21-1 or sh21-2 while *Fbxl3* was knocked down with sh3-1 or sh3-2 as described by Busino et al. (2007). Among them, sh3-2 and sh21-2 abrogated the expression of FBXL3 and FBXL21, respectively, and showed no significant crossover effects with each other (Figure S1A). We found that silencing of the *Fbxl21* gene significantly shortened the period of the cellular rhythm (Figures 2J and S1B). This period-shortening phenotype was not observed in the behavioral rhythms of *Fbxl21*-deficient mice (Figure 2F). Generally, the behavioral rhythms are only marginally affected by molecular defects in clock components due to the strong coupling among the SCN neurons, whereas the phenotypes often become manifest in the circadian rhythms of dispersed cells in culture (Liu et al., 2007). It is likely that the effect of *Fbxl21* deficiency, i.e., speeding up of the molecular oscillation, is masked by the tight neuronal coupling in the SCN. On the other hand, *Fbxl3* knockdown remarkably lengthened the periods, which were conversely shortened by additional knockdown of *Fbxl21* (Figures 2K and S1B). These results are consistent with the behavioral phenotypes of the knockout mice.

Altered Molecular Rhythms in *Fbxl21* Knockout Mice

To investigate how *Fbxl21* deficiency affects the circadian clockwork, we synchronized the cellular clocks in mouse embryonic fibroblasts (MEFs) by a pulse treatment with dexamethasone (Dex). We found that CRY1 and CRY2 protein levels in *Fbxl21*-deficient MEFs were decreased and showed circadian oscillation with reduced amplitudes as compared with those in wild-type MEFs (Figures 3A and 3B). On the other hand, the peak mRNA levels of *Cry1*, *Cry2*, and *Per1* were increased in *Fbxl21* null MEFs (Figure 3C). These results suggest destabilization of CRY proteins in *Fbxl21*-deficient MEFs. In contrast, the mRNA levels of *Dbp* were decreased and *Bmal1* mRNA levels were elevated throughout the day (Figure 3C). Although *Fbxl21*-deficient mice showed rhythmic behaviors with a period indistinguishable from that of wild-type mice (Figure 2C), transcriptional control of the clock genes is remarkably perturbed in the absence of *Fbxl21*. These molecular phenotypes can be at least in part attributable to the dysregulation of CRY1 and CRY2 in *Fbxl21*-deficient cells.

(E) Activity onset in LD cycle. The time of activity onset during the 5 days in LD just before the transition to DD was determined by ClockLab software. The means of the onset times relative to the LD transition time were plotted. Error bars show SEM. *$p < 0.05$ by Tukey's test.

(F) Circadian periods of free-running activities in DD determined by chi-square periodogram. Data from days 8 through 21 in DD were used for the calculation of the circadian periods. Error bars show SEM. *$p < 0.05$ by Tukey's test.

(G) Activity profiles of *Fbxl21*$^{-/-}$ mice across the day. (Upper panel) Typical activity profiles of wild-type and *Fbxl21*$^{-/-}$ mice in DD. (Lower panel) The ratios of the hourly activities relative to the daily total activity in DD of every mouse for each genotype were shown with error bars of SEM. *$p < 0.05$ by Tukey's test. The activity onset time was defined as circadian time 12.

(H) Temporal changes in periodogram amplitude (Qp) of the wheel-running activity rhythms of the knockout mice in DD. The Qp values were determined from the activity data during the four overlapping periods of 8 days in DD (DD1: days 9–16, DD2: days 13–20, DD3: days 17–24 and DD4: days 21–28) by chi-square periodogram by using ClockLab software (Actimetrics). Error bars show SEM. *$p < 0.05$ by one-way ANOVA.

(I) The total numbers of the wheel revolutions per circadian cycle were counted during 2 weeks (days 8–21) in DD. Error bars show SEM, and n.s. indicates not significant ($p > 0.05$ by one-way ANOVA).

(J and K) Circadian periods of cellular rhythms in culture. NIH 3T3 cells were cotransfected with a luciferase reporter (*Bmal1*us0.3-luc; Kon et al., 2008) and shRNA vectors targeting *Fbxl*s (J, *Fbxl21*; K, *Fbxl3* and/or *Fbxl21*). Forty-eight hours after the transfection, the cells were treated with 0.1 μM dexamethasone for 2 hr to synchronize the cellular rhythms. The culture medium was then changed to the recording medium for recording bioluminescence signals. Circadian periods were calculated by using the data from the 2nd to the 4th peak. Error bars show SEM (n = 4, *$p < 0.05$ by Tukey's test). See also Figure S1 and Table S1.

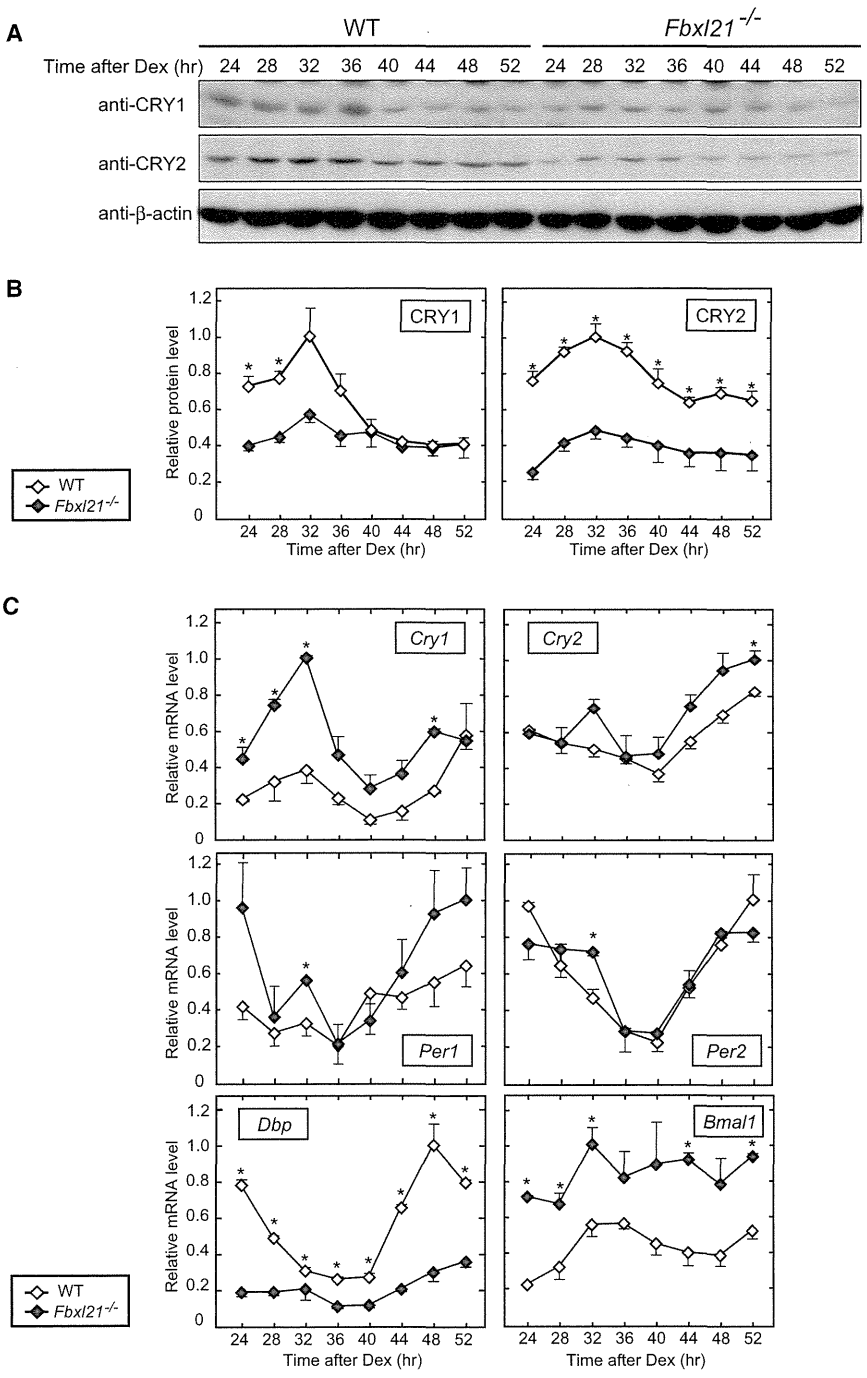

Figure 3. Circadian Expression of CRY Proteins and Clock Genes in *Fbxl21* Knockout Mice

(A) Temporal changes in CRY1 and CRY2 protein levels in *Fbxl21*$^{-/-}$ MEFs. Cellular rhythms of MEFs were synchronized by 2 hr pulse treatment of 0.1 μM dexamethasone. The cells were harvested at 4 hr intervals followed by immunoblotting with CRY1 or CRY2 antibody.

(B) The band densities of CRY1 or CRY2 in (A) within a single blot were shown as values relative to their average intensity in the blot, and the highest value was set at 1.0. Data taken from three independent experiments (i.e. three blots) were averaged and shown with error bars of SEM (n = 3, *p < 0.05 by Student's t test).

(C) Temporal changes in mRNA levels of clock genes in *Fbxl21*$^{-/-}$ MEFs. Cellular rhythms of MEFs were synchronized and total RNA was prepared at 4 hr intervals. The mRNA levels of *Cry1*, *Cry2*, *Per1*, *Per2*, *Dbp*, and *Bmal1* were quantified by real-time PCR, and the highest value among the samples was set at 1.0. Data are means with SEM (n = 3, *p < 0.05 by Student's t test).

ure 4A). The interaction between myc-CRY1 and Flag-FBXL21 was verified by coimmunoprecipitation of myc-CRY1 with Flag-FBXL21 (Figure 4B).

FBXL21 Forms an SCF Complex

Members of the F-box-type E3 ubiquitin ligase family have a conserved F-box domain and a substrate recognition domain that is divergent among the members. The F-box domain is important for the formation of a Skp1-Cul1-F-box protein (SCF) complex to exert E3 ligase activity (Cardozo and Pagano, 2004). To investigate E3 ligase activity of FBXL21, we asked whether FBXL21 forms an SCF complex. Recently, the authors K.Y. and K.I.N. found that FBXL3 forms an SCF complex in a manner dependent on CRY protein (unpublished data). Based on this observation, we coexpressed myc-CRY1 or myc-CRY2 with Flag-FBXL21 or Flag-FBXL3 in HEK293T17 cells. Each myc-CRY facilitated the interaction of Skp1 and Cul1 not only with Flag-FBXL3 but also with Flag-FBXL21 (Figure 4C). It is most likely that FBXL3 and FBXL21 share the same domain for CRY binding and that the E3 ligase activities of these F-box proteins are regulated in a circadian manner through the dynamic change in CRY protein levels. Here, we noticed that Cul1 band in the precipitate with FBXLs was upshifted from the Cul1 band in the input (Figure 4C). Because NEDD8 modification of Cul1 is known to activate the SCF complex by recruiting an E2 enzyme (Pan et al., 2004), the upshifted Cul1 band might

FBXL21 Interacts with CRY Proteins

The abnormalities in temporal changes of CRY1 and CRY2 protein levels in *Fbxl21*-deficient MEFs suggest that FBXL21 shares with FBXL3 a regulatory mechanism determining CRY protein levels. We first examined the interaction of FBXL21 with CRY1 and CRY2 in cultured cells. HEK293T17 cells were transfected with expression constructs of myc-CRYs and Flag-FBXLs. We found that, just like Flag-FBXL3, Flag-FBXL21 was coimmunoprecipitated with myc-CRY1 and myc-CRY2 (Fig-

represent its neddylated state in the SCF complex containing CRYs.

FBXL21 Ubiquitinates CRY Proteins

By using in vitro ubiquitination assay, we examined FBXL21-catalyzed ubiquitination of CRY1 in the presence of 1 of 17 E2 enzymes. We found that UBE2A or UBE2D (D1-D3: UbcH5a-5c) cooperated with not only FBXL3 but also FBXL21 in ubiquitinating CRY1 (Figures 4D and S2A). We also found an in vivo ubiquitination assay that cotransfection of Flag-FBXL3 or Flag-FBXL21 enhanced myc-CRY1 ubiquitination in HEK293T17 cells (Figures 4E and S2B) and NIH 3T3 cells (Figure S2C). Among various linkage types of ubiquitin chains, K48-linked polyubiquitination is primarily known as the protein degradation signal (Behrends and Harper, 2011). The linkage modes of FBXL21- and FBXL3-mediated ubiquitination were examined by using a mutant ubiquitin, HA-K48-Ub, in which all Lys residues except for K48 were mutated to Arg. Coexpression of Flag-FBXL3 or Flag-FBXL21 with HA-wt-Ub promoted myc-CRY1 ubiquitination to be nearly comparable to each other. On the other hand, coexpression with HA-K48-Ub attenuated myc-CRY1 ubiquitination catalyzed by FBXL21 when compared to that achieved with FBXL3 (Figure 4F). These results suggest that FBXL3 and FBXL21 elongate different types of ubiquitin chains, at least in terms of their dependence on K48 linkage. Further studies using a series of other mutant ubiquitins (such as K11-Ub, K48R-Ub, and K63-Ub) would help to identify the linkage mode of ubiquitin chains formed by FBXL21. We then asked whether CRYs are endogenous substrates of FBXL21 in NIH 3T3 cells by knockdown of *Fbxl21*. Silencing of *Fbxl21* or *Fbxl3* reduced the ubiquitinated levels of myc-CRY1 in NIH 3T3 cells (Figures 4G and S2D). These results indicate that CRY1 is an endogenous substrate for FBXL21- and FBXL3-catalyzed ubiquitination.

FBXL21 Stabilizes CRY Proteins

Ubiquitination of proteins confers various regulations on modified proteins, such as protein stability, signal transduction, enzymatic activity, and subcellular localization (Chen and Sun, 2009), whereas F-box protein-mediated ubiquitination predominantly leads the substrates to proteasomal degradation (Cardozo and Pagano, 2004). We asked whether FBXL21 regulates stabilities of CRYs by quantifying the steady-state protein levels of Flag-His-myc-tagged CRY1 (FHM-CRY1) when FBXL21 and/or FBXL3 are either overexpressed or knocked down. Overexpression of Flag-FBXL3 in HEK293T17 cells decreased FHM-CRY1 protein levels, indicating that FBXL3 promotes CRY1 degradation (Figure 5A). In contrast, overexpression of Flag-FBXL21 remarkably elevated FHM-CRY1 levels (Figure 5A). Coexpression of Flag-FBXL3 and Flag-FBXL21 restored FHM-CRY1 levels (Figure 5A), and the restoration was dose dependent for Flag-FBXL21 (Figure 5B). Similar results were obtained in experiments performed with FHM-CRY1 in NIH 3T3 cells (Figure S3A) or with FHM-CRY2 in NIH 3T3 cells (Figure S3B), suggesting that FBXL3 and FBXL21 act on CRY proteins in a mutually antagonizing manner. Myc-PER2 also binds to Flag-FBXL3 and Flag-FBXL21, possibly via indirect interaction through CRYs (Figure S3C), but myc-PER2 protein levels were mostly unaffected by coexpression with Flag-FBXL21 and/or Flag-FBXL3 (Figure S3D). An increase in Flag-FBXL21 levels had no discernible effect on Flag-FBXL3 level (Figures 5A and 5B), eliminating the possibility that the effect of overexpressed Flag-FBXL21 on FHM-CRY1 was due to the change of FBXL3 levels. Meanwhile, knockdown of *Fbxl21* by sh21-2 in NIH 3T3 cells resulted in a decrease in the steady-state levels of FHM-CRY1, whereas knockdown of *Fbxl3* increased FHM-CRY1 levels (Figure 5C). Collectively, these results indicate that CRY1 levels are regulated by FBXL21 and FBXL3 antagonistically, where FBXL21 increases CRY1 levels probably through its stabilization.

To confirm that the stability of CRY proteins is increased by FBXL21, we investigated the degradation rate of myc-CRY1 protein in cultured cells. HEK293T17 cells expressing myc-CRY1 and Flag-FBXLs were treated with cycloheximide (CHX) for 3–6 hr. Expression of Flag-FBXL3 increased myc-CRY1 degradation rate, while Flag-FBXL21 expression significantly suppressed the degradation (Figure 5D). Coexpression of Flag-FBXL3 and FBXL21 attenuated FBXL3-dependent myc-CRY1 degradation. A similar set of experiments in NIH 3T3 cells confirmed the stabilizing effect of Flag-FBXL21 on FHM-CRY1 (Figures S3E and S3F). The half-life of luciferase activity of CRY1-LUC fusion protein was markedly increased (~two-fold) by Flag-FBXL21 expression (Figure 5E), whereas the lifetime of LUC itself was unaffected by Flag-FBXL3 or Flag-FBXL21 (Figure S3G). In *Fbxl21* knockout MEFs, by contrast, the decay of CRY2 was significantly faster than that in wild-type MEFs (Figure 5F). These results demonstrate an important role of FBXL21 in CRY protein stabilization, which antagonizes the destabilizing action by FBXL3.

Ubiquitination Sites in CRY1 and CRY2

We investigated ubiquitination sites in CRY proteins by shotgun proteomic analysis of FHM-tagged CRY1 or CRY2, each of which was immunopurified from the lysates of NIH 3T3 cells (Table 1). We found a series of ubiquitinated residues in FHM-CRYs: K159, K329, and K485 in FHM-CRY1 and K125, K241, K347, K474, and K503 in FHM-CRY2 (Figure 6A, K is labeled with an asterisk). In addition, we found ubiquitinated residues in ubiquitin copurifed with FHM-CRYs: K11, K48, and K63 (Table 1). A recent study of human ubiquitin-modified proteome identified ubiquitinated residues K329 and K442 in CRY1 and K241 and K474 in CRY2 (Kim et al., 2011). The present analysis covered three out of the four ubiquitinated sites reported for human CRYs and revealed two and three additional sites in mouse CRY1 and CRY2, respectively. CRY proteins are multiply ubiquitinated in vivo, suggesting the possibility that FBXL21 and FBXL3 each catalyzes ubiquitination at a distinct subset of Lys residues in CRYs. To examine whether ubiquitination of these sites is essential for FBXL21-mediated stabilization of CRY1, we generated four mutants of myc-CRY1 (mut1–4) by introducing a K-to-R mutation, respectively, at K107, K329, K456, and K485, Lys residues which are ubiquitinated in CRY1 and/or CRY2 and are conserved between CRY1 and CRY2 (Figure 6A). Among these mutants, mut1-CRY1 (K107R) protein levels were sensitive to FBXL3-dependent degradation and, by contrast, they were unaffected by coexpression of FBXL21 in

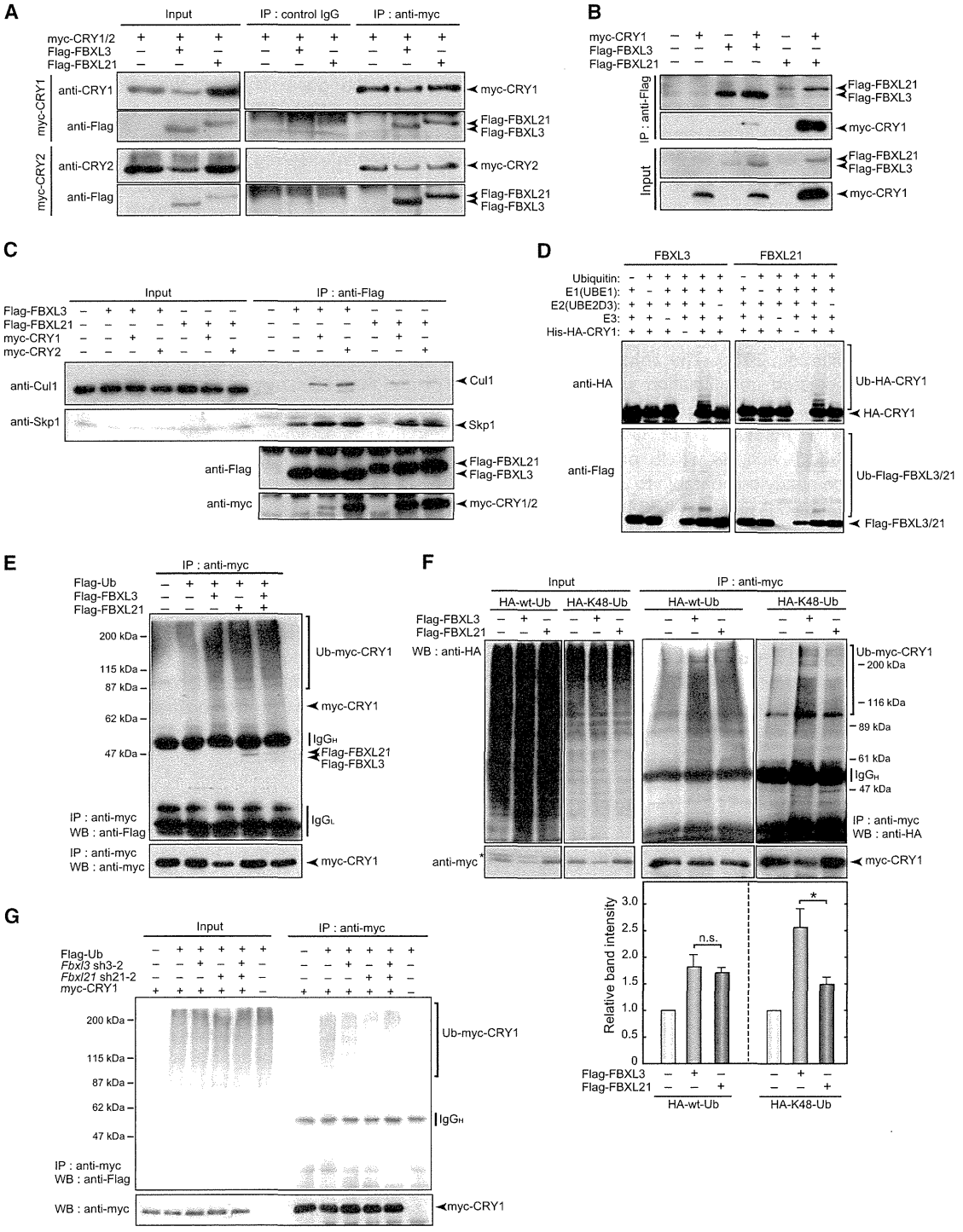

Figure 4. Interaction of FBXL21 with CRY1 and CRY2

(A) Interaction of FBXL21 with CRY1 and CRY2 in HEK293T17 cells. Cells were transfected with myc-CRYs and Flag-FBXL3 or Flag-FBXL21 expression vectors. Forty-eight hours after the transfection, the cells were harvested and lysed in IP buffer, followed by immunoprecipitation with anti-myc antibody. Immunoprecipitated product was analyzed with anti-Flag antibody.

(B) Myc-CRY1 and Flag-FBXL3 or FBXL21 were expressed in HEK293T17 cells and Flag-FBXLs were immunoprecipitated with anti-Flag antibody. Interaction of FBXL3 or FBXL21 with myc-CRY1 was detected with anti-myc antibody.

(C) FBXL21 forms SCF complex with CRY proteins. Flag-FBXLs and myc-CRY1 expression constructs were transfected into HEK293T17 cells. Interaction of FBXL21 with endogenous Cul1 and Skp1 were detected with anti-Cul1 and anti-Skp1 antibody.

(legend continued on next page)

HEK293T17 cells (Figures 6B and 6C). The other three mutant proteins (mut2–4) were mostly sensitive to both FBXL3-dependent degradation and FBXL21-dependent stabilization (Figures 6B and 6C). These observations suggest that FBXL21 stabilizes CRY1 through ubiquitination of at least one unique Lys residue K107, which is not involved in FBXL3-dependent degradation.

Subcellular Localization of FBXL21

Although the amino acid sequences of FBXL21 and FBXL3 are highly conserved, their N-terminal regions are divergent from each other. We found in this region a putative nuclear localization signal (NLS) sequence KRPR only in FBXL3 (Figure 6D). Interestingly, the NLS sequence at the corresponding position of FBXL21 is disrupted by amino acid insertion (Figure 6D). To reveal the spatial regulation of CRY ubiquitination, we examined subcellular distribution of FBXL21, FBXL3, and NLS-mut-FBXL3 that have mutations KRPR-to-AAAA at positions 22–25. Flag-FBXL3 was localized predominantly to the nucleus of HEK293T17 cells as reported by Godinho et al. (2007), whereas NLS-mutated Flag-FBXL3 was detected in the cytosol (Figures 6E and 6F), indicating that the NLS sequence is critical for nuclear localization of FBXL3. In contrast, Flag-FBXL21 was found in the cytosol with weak distribution in the nucleus (Figures 6E and 6F). Such a contrast in distribution suggests that CRY stabilities are regulated by FBXL21 and FBXL3 predominantly at different subcellular spaces. To reveal an impact of FBXL21 on nuclear and cytosolic CRYs, we investigated CRY levels in these two fractions of the mouse brain lysate prepared at ZT18 from *Fbxl3*, *Fbxl21*, and *Fbxl3/Fbxl21* knockout mice. As compared to wild-type, *Fbxl21*-deficient mice showed reduced levels of CRY1 and CRY2 in both the cytosol and the nucleus (Figures 6G and 6H). In *Fbxl3* null background, on the other hand, *Fbxl21* knockout decreased CRY levels only in the cytosol (Figure 6H). These findings suggest that FBXL21 protects CRYs from FBXL3-mediated degradation in the nucleus, where a minor population of FBXL21 is located. The results also imply that at least one additional CRY degradation system is operating in the cytosol, where FBXL21 plays a major role for CRYs stabilization. It is probable that the finely tuned accumulation of CRY proteins in the cytosol mediated by FBXL21 in combination with another degradation mechanism determines the proper timing of their nuclear entry (Figure 6I).

DISCUSSION

In the present study, we provide evidence for the physiological role of *Fbxl21* in the regulation of the circadian clockwork. FBXL3 and FBXL21 each bind with CRY1 and CRY2 (Figures 4A and 4B) and form an SCF complex (Figure 4C), which mediates ubiquitination of CRY proteins (Figures 4D, 4E, and 4G). Intriguingly, FBXL3 and FBXL21 regulate the stability of CRY proteins in opposite directions despite the high degree of their sequence identity (Figure 5). We found that the K-to-R mutation in CRY1 at K107, one of the ubiquitination sites identified in the present study (Table 1), attenuates FBXL21-dependent stabilization and, by contrast, has no significant effect on FBXL3-dependent degradation (Figures 6B and 6C). FBXL21 may exert its stabilizing effect on CRYs through ubiquitination of K107 in CRY1 and the corresponding residue K125 in CRY2. A CRY1 peptide, having ubiquitinated K107, was not detected in our shotgun proteomic analysis, but we speculate that substantially low ubiquitinated levels of CRY1 in NIH 3T3 cells could have hampered its detection. The Lys residues at these positions are conserved in CRY1 and CRY2 from a wide range of species, including humans, chickens, zebrafish, *Xenopus*, and Anole lizards (http://www.ensembl.org/), and CRY1 and CRY2 show the high degree of amino acid identity at the surrounding sequences, raising the possibility that K107 is a common site for ubiquitination among vertebrate CRYs in vivo.

It is well established that F-box protein-mediated ubiquitination of proteins leads to their proteasome-dependent degradation (Pan et al., 2004; Frescas and Pagano, 2008). The only reported exception to this paradigm is the stabilization of c-Myc by β-TrCP-mediated polyubiquitination, which interferes with FBXW7-mediated c-Myc ubiquitination that leads to its degradation (Popov et al., 2010). β-TrCP and FBXW7 competitively ubiquitinate the same residue on c-Myc and conjugate different linkage types of polyubiquitin chains. In this way, β-TrCP-mediated polyubiquitination protects c-Myc against FBXW7-mediated ubiquitination and degradation, and accordingly, β-TrCP is effective only in the presence of FBXW7. In the case of CRY proteins, it is likely that FBXL3 catalyzes elongation of K48-linked polyubiquitin chain, whereas FBXL21 appears to elongate a different type of ubiquitin chain (Figure 4F). In fact, we detected K11- and K63-linked structures in ubiquitins copurified with CRY proteins (Table 1). Our findings suggest FBXL21-mediated formation of a polyubiquitin chain with a K11- or K63-linked mode or a mode comprising a combination of K11, K63, or K48 linkage. CRY proteins are probably stabilized by a mechanism in which the ubiquitination of CRYs catalyzed by SCF^{FBXL21} could either compete with the formation of the K48-linked polyubiquitin chain (the degradation signal) or interfere with the function of the degradation signal.

Here, we emphasize that the phenotypes of *Fbxl21* ablation are observed even in the absence of *Fbxl3* at the behavioral level (Figure 2F) and at the molecular level (Figures 5C and 6H). These observations strongly suggest additional regulation of degradation-stabilization of CRYs operating in the cytosol, which is

(D) In vitro ubiquitination assay of CRY1. Recombinant ubiquitin, E1, E2 (UBE2D3), Rbx1, Skp1-Cul1-FBXLs (SCF^{FBXLs}), and HA-CRY1 were incubated for 2 hr at 30°C. Ubiquitinated HA-CRY1 (Ub-HA-CRY1) was detected by immunoblotting with anti-HA antibody.

(E) In vivo ubiquitination assay of CRY1. Flag-ubiquitin (Ub), myc-CRY1, and Flag-FBXLs were expressed in HEK293T17 cells. Forty-two hours after the transfection, the cells were treated with 10 μM MG132 for 6 hr. Ubiquitination of myc-CRY1 purified with anti-myc antibody was detected by anti-Flag antibody.

(F) In vivo ubiquitination assay of CRY1. HA-wt-Ub or HA-K48-Ub was coexpressed with myc-CRY1 and Flag-FBXLs in HEK293T17 cells. Forty-two hours after the transfection, the cells were treated with 10 μM MG132 for 6 hr. Ubiquitination of myc-CRY1 purified with anti-myc antibody was detected by anti-HA antibody. The intensity of the smeared bands of polyubiquitinated CRY1 was quantified. Data are means + SEM (n = 3, *p < 0.05 by Student's t test).

(G) *Fbxl21* knockdown reduced CRY1 ubiquitination. shRNA expression vectors targeting *Fbxl*s were transfected to NIH 3T3 cells and the cells were treated with 10 μM MG132 for 6 hr before harvest. Ubiquitination of myc-CRY1 purified with anti-myc antibody was detected by anti-Flag antibody. See also Figure S2.

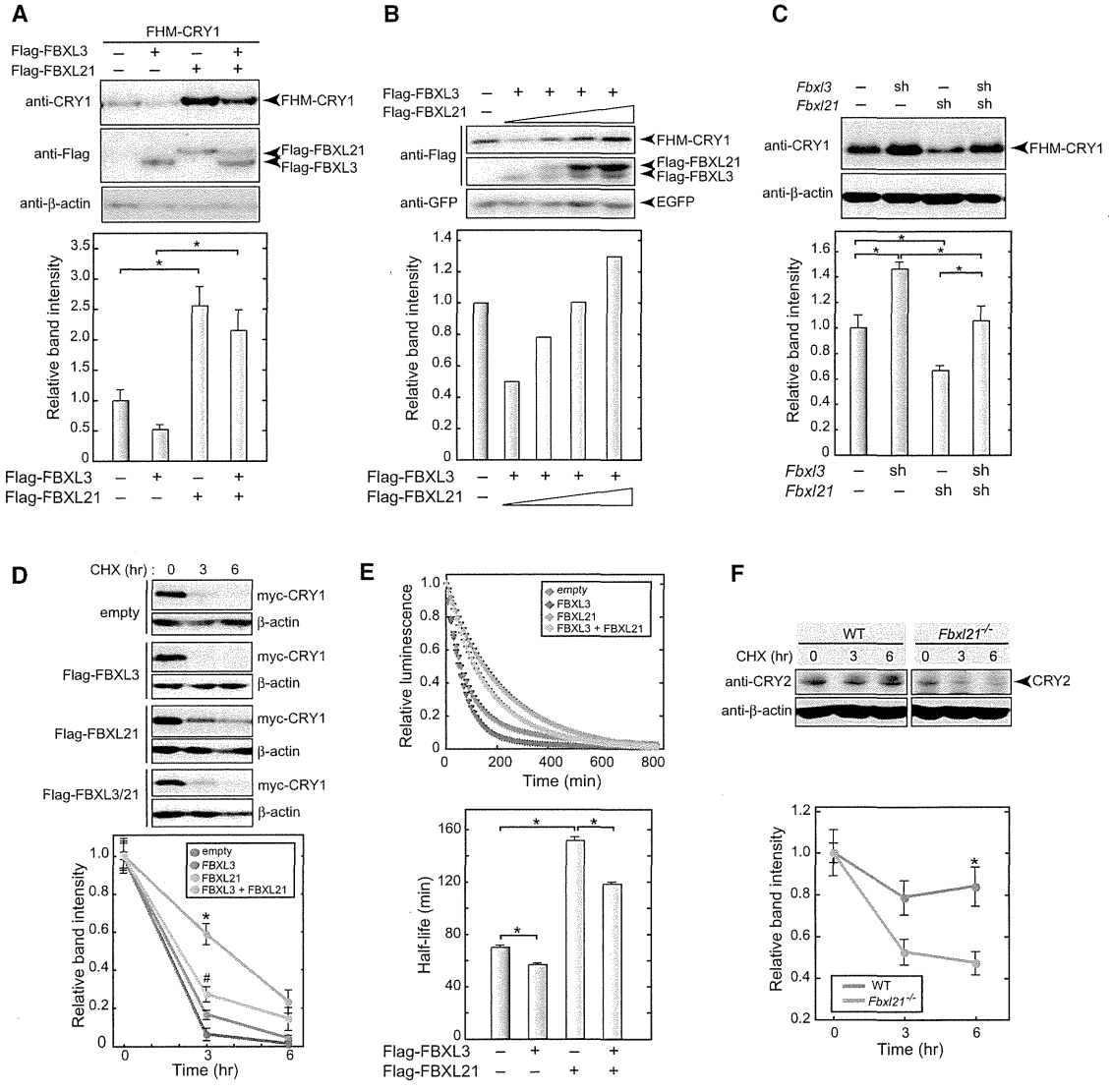

Figure 5. Effect of FBXL21 on the Stability of CRY Proteins

(A) Effect of FBXL21 on the steady-state levels of CRY1 protein. Flag-His-myc-CRY1 (FHM-CRY) and Flag-FBXL expression vectors were cotransfected to HEK293T17 cells. Forty-eight hours after the transfection, CRY1 expression levels were quantified by immunoblotting with CRY1 antibody. Data are means + SEM (n = 3, *p < 0.05 by Tukey's test).

(B) FBXL21 dose dependently restored CRY1 protein levels that were reduced by FBXL3. The amounts of the plasmid for Flag-FBXL21 expression were 0, 50, 100, and 200 ng. EGFP was used for a loading control.

(C) Effect of *Fbxl21* knockdown on the steady-state levels of CRY1 protein. shRNA expression vectors (sh3-2 or sh21-2) were transfected to NIH 3T3 cells. Seventy-two hours after the transfection, CRY1 levels were quantified by immunoblotting with CRY1 antibody. Data are means + SEM (n = 3, *p < 0.05 by Tukey's test or Dunnett's test).

(D) Degradation assay of myc-CRY1. Flag-FBXLs and myc-CRY1 were expressed in HEK293T17 cells. Forty-eight hours after the transfection, the cells were treated with 100 μg/ml CHX for 3 or 6 hr. Then, the cells were harvested, followed by immunoblotting with CRY1 antibody. CRY1 levels at time zero in each condition were normalized to 1.0. Data are means + SEM (n = 3; *p < 0.05 by Tukey's test between empty and FBXL21; #p < 0.05 by Tukey's test between FBXL3 and FBXL3+FBXL21).

(E) Degradation assay of CRY1-LUC. CRY1-LUC and Flag-FBXLs were expressed in HEK293T17 cells. Forty-eight hours after the transfection, bioluminescence levels were monitored in the recording medium containing CHX. Half-life of CRY1-LUC was calculated by fitting the data with an exponential function and shown with error bars of SEM (n = 4, *p < 0.05 by Tukey's test).

(F) Degradation assay of endogenous CRY2 in *Fbxl21*$^{-/-}$ MEFs. MEFs were treated with CHX for 3 or 6 hr and then harvested, followed by immunoblotting with CRY2 antibody. The protein levels at time zero in each genotype were normalized to 1.0. Data are means + SEM (n = 3, *p < 0.05 by Student's t test). See also Figure S3.

Table 1. Ubiquitination Sites Identified by Shotgun Proteomic Analysis

Protein[a]	Position	Ubiquitinated Peptide[b]
CRY1		
	153–177	FQTLVSK$_{159}$MEPLEMPADTITSDVIGK
	323–334	NPEALAK$_{329}$WAEGR
	484–493	MK$_{485}$QIYQQLSR
CRY2		
	114–127	LTFEYDSEPFGK$_{125}$ER
	239–245	LDK$_{241}$HLER
	341–352	NPEALAK$_{347}$WAEGK
	461–477	YIYEPWNAPESVQK$_{474}$AAK
	502–511	MK$_{503}$QIYQQLSR
Ubiquitin		
	7–27[c]	TLTGK$_{11}$TITLEVEPSDTIENVK
	43–54[d]	LIFAGK$_{48}$QLEDGR
	55–72[d]	TLSDYNIQK$_{63}$ESTLHLVLR

[a]FHM-CRY1, FHM-CRY2 or FH-LacZ purified from NIH 3T3 lysate was subjected to shotgun proteomic analysis (see Extended Experimental Procedures for details).
[b]Glycylglycine was found to be linked via an amide bond to the epsilon amino group of the lysine residue (K) underlined. These residues were assigned as the attachment sites of ubiquitin because glycylglycine is derived from its C-terminal sequence RGG after proteolysis with trypsin.
[c]A peptide detected from the analysis of CRY2.
[d]Peptides detected from the analyses of both CRY1 and CRY2.

obviously different from the dual regulation by FBXL21 and FBXL3 in the nucleus. FBXL21-mediated stabilization and the counterbalancing degradation of CRYs in the cytosol are critical for determining the accumulation rate of CRY proteins. We previously reported a CRY2 degradation mechanism dependent on Ser557/Ser553 phosphorylation in the cytosol (Kurabayashi et al., 2010). However, the binding affinity of CRY2 to FBXL21 was unaffected by S557A mutation, and S557A-CRY2 protein levels were increased by coexpression of FBXL21 (data not shown). Thus, FBXL21 is less likely to be involved directly in Ser557/Ser553 phosphorylation-dependent degradation of CRY2. Multiple ubiquitination sites in CRY1 and CRY2 (Table 1) are indicative of a complex network of CRY ubiquitination that is important for the circadian clockwork.

Fbxl21 knockout mice showed wheel-running rhythms in DD with a period indistinguishable from that of their wild-type littermates (Figure 2F). On the other hand, the Takahashi laboratory (UT Southwestern, USA) found a point mutation in FBXL21 that causes a shortened period of behavioral rhythms (Yoo et al., 2013, this issue of *Cell*). This short-period phenotype is consistent with our observation on the cellular clock, in which silencing of *Fbxl21* in NIH 3T3 cells significantly shortened the period (Figure 2J). We speculate that *Fbxl21* slows down the oscillation speed and that the difference in phenotypes of *Fbxl21* ablation between behavioral and cellular rhythms (Figures 2F and 2J) may be explained by consolidation of the circadian oscillation in the SCN (Liu et al., 2007). It is noteworthy that *Fbxl21* null mice showed a decrease in wheel-running activities near the subjective dawn (Figure 2G). Thus, *Fbxl21* deficiency appears to also affect the SCN clock function regulating the temporal organization of the behaviors. The profound and complex perturbations in the circadian expression profiles of the clock genes (Figure 3C) might be responsible for this abnormality, though the underlying mechanism has yet to be elucidated.

Fbxl21 knockout in *Fbxl3* null background significantly shortened the long circadian period of the behavioral rhythm of *Fbxl3* null mice (Figure 2). This result can be explained by the antagonizing effects of FBXL21 and FBXL3 on CRY stabilities. Importantly, despite the apparent alleviation of the abnormalities of *Fbxl3* knockout mice in terms of the circadian period and the activity onsets, *Fbxl3*/*Fbxl21* double-knockout mice exhibited unstable circadian behaviors as revealed by the occurrence of arrhythmic mice in DD (three out of ten mice; Figure 2D and Table S1) and by the progressive decline in the periodogram amplitude (Qp) during days 9–28 in DD (Figure 2H). Qp is a measure of robustness of circadian rhythms (Sokolove and Bushell, 1978), and the values were unaltered in *Fbxl3* and *Fbxl21* single-knockout mice in DD (Figure 2H). We conclude that FBXL21 and FBXL3 cooperatively play an essential role for the maintenance of the robust clock oscillation by providing a mechanism counterbalancing CRY1 and CRY2 protein levels.

Here we propose a model in which CRY proteins are regulated by FBXL21 and FBXL3 so as to maintain normal circadian oscillation (Figure 6I). FBXL21-mediated ubiquitination of CRY1 and CRY2 provides an ~12 hr time window for accumulation of CRY proteins in the cytosol when the E-box-dependent transcription is kept active. This idea is supported by the subcellular distribution of FBXL21 (Figure 6E) and by the marked reduction of CRY levels in *Fbxl21*-deficient cells (Figures 3B and 6H). *Fbxl21* transcripts show marked circadian variations in the mouse SCN (Dardente et al., 2008), and *Fbxl21* mRNA levels are high during the mid- to late-subjective day when *Cry1* and *Cry2* mRNA levels increase. It is most likely that FBXL21 plays an important role for temporally organizing the accumulation of translated CRYs in the cytosol. On the other hand, FBXL3 ubiquitinates CRYs predominantly in the nucleus to terminate suppression of the E-box-dependent transcription (Godinho et al., 2007). Collectively, a spatiotemporally fine-tuned balance between stabilization and degradation mediated by FBXL21 and FBXL3, respectively, is essential for coordinating the ~24 hr variation of protein abundance of CRY1 and CRY2, the key players in the transcription-based autoregulatory feedback in the circadian clock.

Ubiquitination-mediated degradation of clock proteins, especially that of the transcriptional repressors, has been highlighted as a key regulatory process in the clockwork of many organisms (Gallego and Virshup, 2007; Baker et al., 2012; Ito et al., 2012). In the present study, we demonstrate that coordination of a destabilizer, FBXL3, with a stabilizer, FBXL21, each acting antagonistically on CRY repressors, is critical for generating the CRY expression dynamics and behavior rhythms. CRY protein levels are critical determinants of the timing of CLOCK-BMAL1-dependent transcriptional activation. Thus, the balance between CRY stabilization and degradation mediated by a combination of FBXL21 and FBXL3 is essential to drive the 24 hr cycle of the circadian clock. Our results underscore an emerging concept that switching between protein degradation and stabilization